Report
**R-15-01**
September 2017

# Concept testing and site-scale groundwater flow modelling of the ice sheet marginal-area of the Kangerlussuaq region, Western Greenland

**Patrik Vidstrand**

SVENSK KÄRNBRÄNSLEHANTERING AB

SWEDISH NUCLEAR FUEL
AND WASTE MANAGEMENT CO

Box 3091, SE-169 03 Solna
Phone +46 8 459 84 00
skb.se

SVENSK KÄRNBRÄNSLEHANTERING

ISSN 1402-3091
**SKB R-15-01**
ID 1493455
September 2017

# Concept testing and site-scale groundwater flow modelling of the ice sheet marginal-area of the Kangerlussuaq region, Western Greenland

Patrik Vidstrand, TerraSolve AB

# Abstract

As a part of the Greenland Analogue Project (GAP), the Swedish Nuclear Fuel and Waste Management Company (SKB) and Posiva have undertaken a series of groundwater flow modelling studies. These represent different scales and address different sub-objectives under the same overall modelling objective to: *investigate the conditions and processes that impact the recharge of glacial melt water into the geosphere, in particular to repository depth in a fractured crystalline rock and over safety assessment time scales.* The groundwater flow modelling work reported here comprises a coupled thermal-hydraulic (T-H) analysis of the GAP study area in western Greenland.

The objective of this report is to provide insight into the relevance of traditional assessments specified pressure top boundary condition, and to make detailed examination of specific areas of the GAP study site. The modelling is accompanied by a sensitivity study to address the impact of the following issues: different representations of a sub-glacial transmissive layer at the interface between the ice sheet and the geological substratum, the applied specified pressure top boundary, and the amount of sub-glacial permafrost.

The main conclusions of this work are that for simulations of deep groundwater systems specified pressure top boundaries are valid and useful. However, in order to assess simplified top boundary conditions in a relevant fashion, proper representation of local topography as well as sub-glacial permafrost are important. To reveal details of sub-glacial groundwater flow and melt water transport within a transmissive layer, proper model resolution is essential. Upscaling this transmissive layer is problematic, if possible. Talik lakes in the periglacial environment are found to be discharge zones for glacial melt water; however, different locations within the same talik may concurrently provide recharge to the deeper groundwater system.

# Sammanfattning

Som en del av Greenland Analogue Project (GAP), har Svensk Kärnbränslehantering AB (SKB) och Posiva Oy (Posiva) genomfört en serie grundvatten flödesstudier. Dessa representerar olika skalor och olika delmål under samma övergripande modelleringmål; att utreda förutsättningarna och processer som påverkar nedträngningen av glacialt smältvatten i geosfären, särskilt till förvarsdjup i en sprickig kristallin berggrund över säkerhetsanalystider.

Grundvattenflödesmodelleringsstudien som redovisas här omfattar en kopplad termohydraulisk (TH) analys av delar av GAPs fältområde.

Syftet med rapporten är att ge en inblick i betydelsen av traditionellt använt specificerade trycktopprandvillkor och att i detalj studera vissa fokuserade områden i GAP:s fältområde. Arbetet inkluderar en känslighetsstudie som behandlar effekterna av bland annat följande frågor: olika representationer av ett sub-glacialt transmissivt lager vid gränsytan mellan inlandsisen och det geologiska underlaget, det tillämpade specificerade tryckrandvillkoret, och utbredningen av sub-glacial permafrost.

Den viktigaste slutsatsen är att för simuleringar av djupa grundvattensystem är specificerade trycktopprandvillkor giltiga och användbara. Emellertid, vid användning av förenklade topprandvillkor på ett relevant sätt är lokal topografi såväl som sub-glacial permafrost viktiga faktorer. Vid behov av mer information om ytligt sub-glacialt grundvattenflöde och smältvattentransport inom ett transmissivt lager föreligger ett behov av högupplösta modeller. Uppskalning av detta transmissiva lager är komplicerat om ens möjligt. Talikar inom det periglacial området representerar utflöde av glacialt smältvatten; men kan också, och samtidigt, men på andra delar av samma talik bilda nytt grundvatten för det djupare grundvattensystemet.

# Contents

# 1 Introduction

## 1.1 Background

Site investigations with subsequent performance or safety assessment studies for the location of deep, geological repositories designed for long-term storage of spent nuclear fuel are on-going, on different levels, in e.g. Sweden, Finland, and Canada. These studies are undertaken by SKB, Posiva, and NWMO, respectively. At all locations available for these organizations, future periglacial and glacial climate conditions are expected. At least in Sweden and Finland, however, no ice sheets currently exist, with present climate producing only small cirque and valley glaciers in mountainous areas and no extensive permafrost.

As an analogue to future extensive ice sheets, the Greenland Ice Sheet (GrIS) and the periglacial area in front of the ice sheet in a region east of Kangerlussuaq was chosen to provide field data for use in the multilateral Greenland Analogue Project (GAP), initiated and funded by SKB, Posiva, and NWMO (cf. Figure 1-1). Parallel to the GAP, modelling studies were conducted incorporating modelling teams from different scientific areas, i.e. ice sheet modellers, hydrological and groundwater flow modellers.

The GAP study area is mainly located between the Isunnguata Sermia outlet glacier to the north, and the Russell outlet glacier to the south, but work has also been conducted in front of the Leverett outlet glacier (see Figure 1-2). The groundwater models developed in relation to the GAP have a spatial focus on the hydrologic responses of the three outlet glaciers and the surroundings of the DH-GAP04 borehole, as well as on responses in a Talik lake.

The results from the GAP are in detail described in Harper et al. (2016) and Claesson Liljedahl et al. (2016).

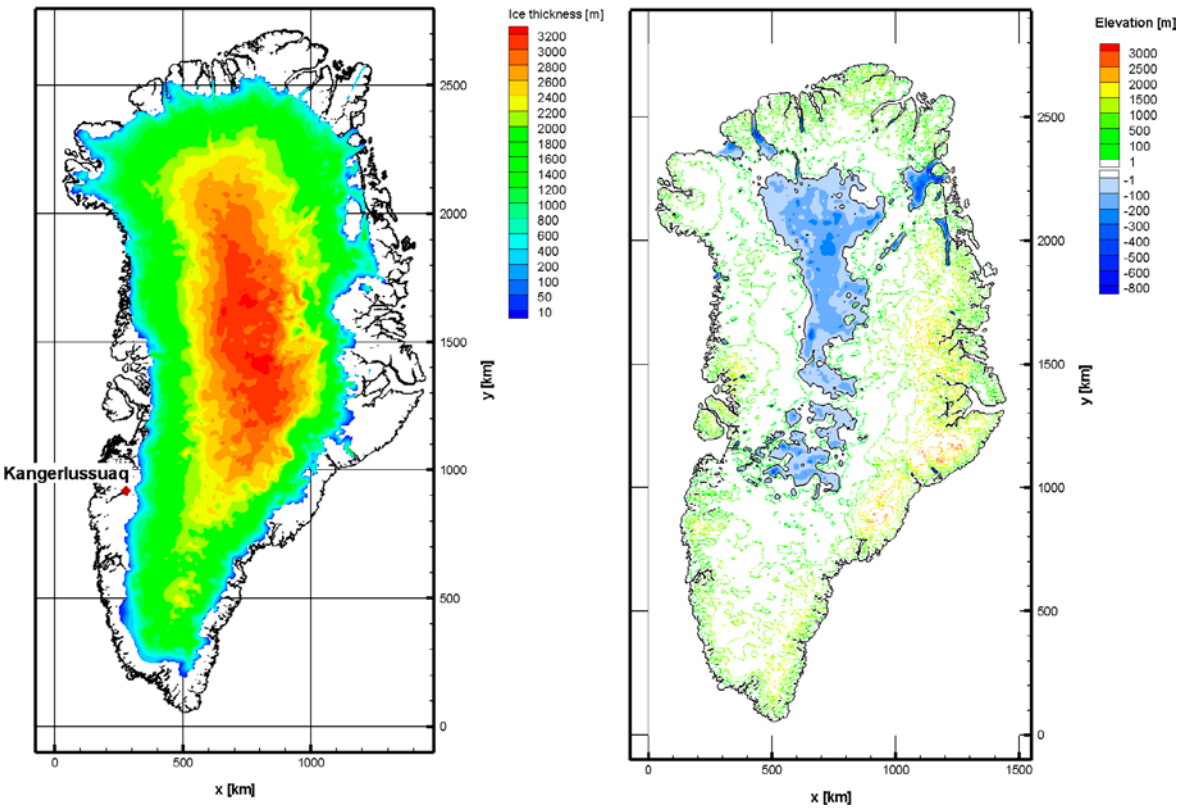


***Figure 1-1.*** *Location of Kangerlussuaq on the west coast of Greenland. The figure illustrates (left) the ice sheet thickness and (right) the ground surface elevation of Greenland. The data used for interpolation is the Bamber 1993–1999 data set available at the "National Snow and Ice Data Centre", http://nsidc.org/data/nsidc-0092.html.*

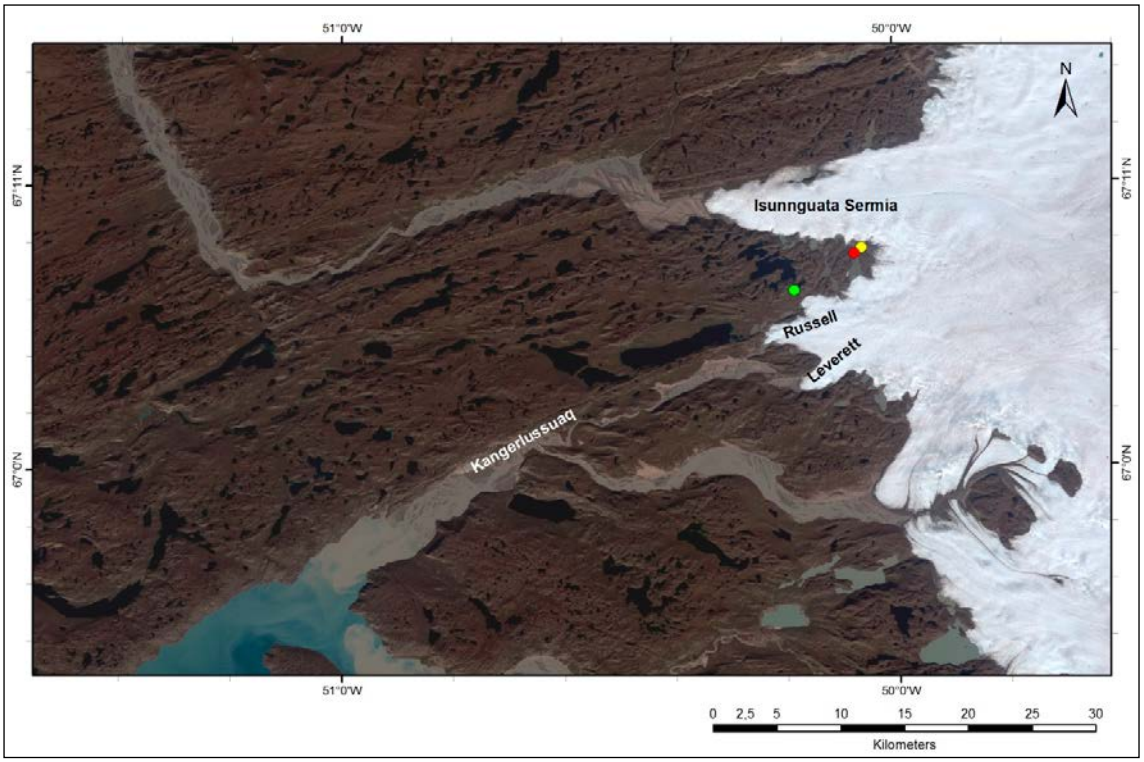


***Figure 1-2.*** *Overview of part of the GAP study area. The DH-GAP04 borehole (yellow) is a cored borehole drilled, monitored and maintained by the GAP. The DH-GAP01 borehole (green) was drilled in under the Talik lake to study talik processes. The DH-GAP03 borehole (red) was drilled to obtained information about permafrost depth close to the ice margin. Background image is a Landsat image acquired 23 August, 2000.*

The present report summarises the work related to a groundwater flow modelling study of the GAP site. The following section and subsequent chapters are organized as follows:

- Chapter 1 presents the scope, objectives and a brief discussion on relevant background information for understanding the problem and the study area.
- Chapter 2 presents the basis for the developed conceptual ideas; the chapter is based on information from a literature review.
- Chapter 3 presents assessed concepts and the mathematical background of the DarcyTools code.
- Chapter 4 presents the data gathering, processing and assessment along with the results and discussions of the results.
- Chapter 5 provides conclusions and provides recommendations for future work.

## 1.2 Objectives

The aim of the work in the present report is to investigate effects of small to local scale variability, and from that hopefully provide modelled feed-back to the field experiments and constraints for the large scale models concerning the need to resolve the interface between the ice sheet and the bedrock.

The objective of the GAP geosphere modelling is to *investigate the conditions and processes that impact the recharge of glacial melt water into the geosphere, in particular to repository depth in a fractured crystalline rock and over safety assessment time scales.* Specifically, it is the recharge of dilute and oxygenated glacial melt waters to repository depth that is of most relevance since these waters pose a risk to the engineered barriers of the repository system (Fischer et al. 2015).

The modelling in the present report takes two different approaches to investigating the glacial environment. The first approach (Part I) is to:

- investigate the influence of recharge variations on groundwater flow and pressure in a sub-glacial environment, and
- investigate the relevance of the top boundary conditions usually used in large scale groundwater flow models', i.e. in general, a specified pressure condition.

The second approach (Part II) differs in that sensitivity studies are performed on the traditional type of top boundary conditions relevant for areas with sub-glacial permafrost, i.e. specified pressure. In this context the analyses are aimed at:

- providing a first set of supporting indications of regional recharge and discharge characteristics of the Talik Lake site, and
- investigating the flow and pressure system in the region around the DH-GAP04 cored borehole.

## 1.3 Conceptual model

A literature review (presented in Chapter 2) was undertaken with the objective of justifying hydraulic properties and boundary conditions of a groundwater flow model intended for hydraulic, thermal and chemical modelling during periglacial (permafrost) and glacial conditions. The conceptual model motivating the applied hydraulic properties and hydraulic top boundary conditions used are summarised below.

In front of the ice sheet margin, the surface freezes because of low air temperatures. In the simulations that consider glacial conditions with permafrost, the freezing propagates into the subsurface thus altering flow and transport properties. A freezing algorithm (presented in Chapter 3) is used to modify the initial permeability values.

In Part I, a distributed recharge of melt water beneath the ice sheet is assumed, whereas in Part II an infinite source of melt water with a hydraulic head at the base of the ice sheet equal to 30–92 % of the ice sheet thickness is assumed. Furthermore, in Part II a permafrost wedge with varying extent, stretching in beneath the ice sheet, is assumed. The imposed boundary condition, both in Part I and in Part II, implies that sub-glacial melt water infiltrates the subsurface and flows from areas with high hydraulic heads to areas with lower hydraulic heads where it discharges. The simulated discharge locations vary in space depending on the characteristics of the particular simulation. Likely locations of so-called taliks[1], which may act as either recharge or discharge locations, are estimated from a digitalized lake map of the GAP study area.

The GAP study area is in this work assumed to be well represented by hydraulic and mechanical properties similar to those of the typical bedrock in Sweden. This implies a low mechanical loading efficiency; hence a small or no delay in pressure responses are expected, and small or no changes in the storage of water in the flowing fracture system are expected in response to changes at the top boundary during glaciation and deglaciation. Furthermore, a low mechanical loading efficiency is also considered appropriate given the objective of the present work; this is due to the fact that a low loading efficiency increases the hydraulic gradients imposed and thereby also the Darcy fluxes and associated chemical changes at repository depth. Assuming a zero loading efficiency, i.e. no mechanical coupling, implies that the classic hydraulic mass balance equation for transient groundwater flow is applied.

Neglecting mechanical coupling is a valid assumption for cases when sub-glacial pressure is around 92 % of the ice thickness. For the sensitivity cases in Part II with lower pressure levels than 92 %, e.g. 30 % and 70 %, the assumption is more questionable, this since a lower hydraulic pressure than 92 % along with the same ice overburden creates changed effective stress conditions in the subsurface.

[1] Taliks are unfrozen "holes" in the permafrost layer that can connect the flow system at depth with that closer to the surface.

For the sake of clarity, the potential hydraulic impact of an uneven surface loading in proximity to the ice sheet margin (generally known as crustal flexure or the forebulge phenomenon) is not addressed in the work reported here. Finally, sub-glacial runoff through structures embedded in the ice sheet or occurring at the ice sheet-bedrock interface, e.g. sub-glacial melt water tunnels are not considered here.

## 1.4 Setting of the GAP study area

The groundwater flow model presented in Part I focuses on the Russell and Leverett outlet glaciers, whereas the Part II model also incorporates the Isunnguata Sermia outlet glacier.

It is worth noting that from a hydraulic point of view the entire GAP study area assessed herein is in the region of the ice sheet that is the edge of the ice sheet and as such the ice gradients and hence associated groundwater gradients are steeper than the interior of the ice sheet.

Further details on the study area can be found in Wallroth et al. (2010).

### 1.4.1 Deglaciation

About 7 000 year BP, the retreating ice front had reached Kangerlussuaq, and by 6 000 year BP it had reached its present day position (Kelly 1985, van Tatenhove et al. 1996). It is unknown how far to the east the ice front retreated, but by comparing different deglaciation dates from the moraine system before 6 000 year BP, van Tatenhove et al. (1996) infer that the ice reached 10's of kilometres beyond the present-day ice front. Neoglacial advances started at 4 000 year BP (e.g. Kelly 1985, Willemse and Törnqvist 1999, Anderson et al. 1999, Bennike 2000) and ended AD 1700–1920, during the Little Ice Age as indicated by moraines near the position of the present day ice front (Weidick 1968). Both Neoglacial and Little Ice Age limits occur within 2 km of the present-day ice margin (Forman 2008).

### 1.4.2 Climate

The climate in Greenland is predominantly arctic. The region around Kangerlussuaq is dominated by the ice sheet, but along its margin, a periglacial domain dominates the landscape. The periglacial domain consists of an arctic mountain landscape which is characterised by low vegetation.

There is a strong climatic gradient between the coast and the western margin of the Greenland ice sheet. While winters at the coast are characterised by a relatively thick snow cover, there is generally little snow at Kangerlussuaq. At Sisimiut, some 130 kilometres to the west at the coast, the average annual temperature is –3.9 °C while at Kangerlussuaq, where there is a more continental climate, the average annual temperature is –5.7 °C. The area at the head of the fjord is characterised by continuous permafrost and low precipitation. The zone closest to the ice sheet has a very low (or even negative) effective precipitation.

### 1.4.3 Geology

The Nagssugtoqidian Orogen of West Greenland represents a Palaeoproterozoic tectonic belt with prominent ENE-trending foliation. It is situated between the North Atlantic Craton to the south and the Archaean craton that includes Rinkian Orogen to the north.

Engström et al. (2012) produced a "Geomodel" for the GAP study area that utilised at the time all available information (geological, topographical and geophysical). The modelled area was divided into two scales: 1) a regional-scale area and 2) a site-scale area as shown in Figure 1-3. The GAP site scale refers to the area where surface mapping has been performed, and where DH-GAP01, DH-GAP03 and DH-GAP04 were drilled during the GAP project.

The "Geomodel" includes processed mapped data collected by the GAP during 2008–2010, and the analysis of fracture data from the pilot boreholes holes (DH-GAP01 and DH-GAP03) drilled in 2009. The "Geomodel" is a 2D model with a total of 158 deformation zones/faults, see Figure 1-4.

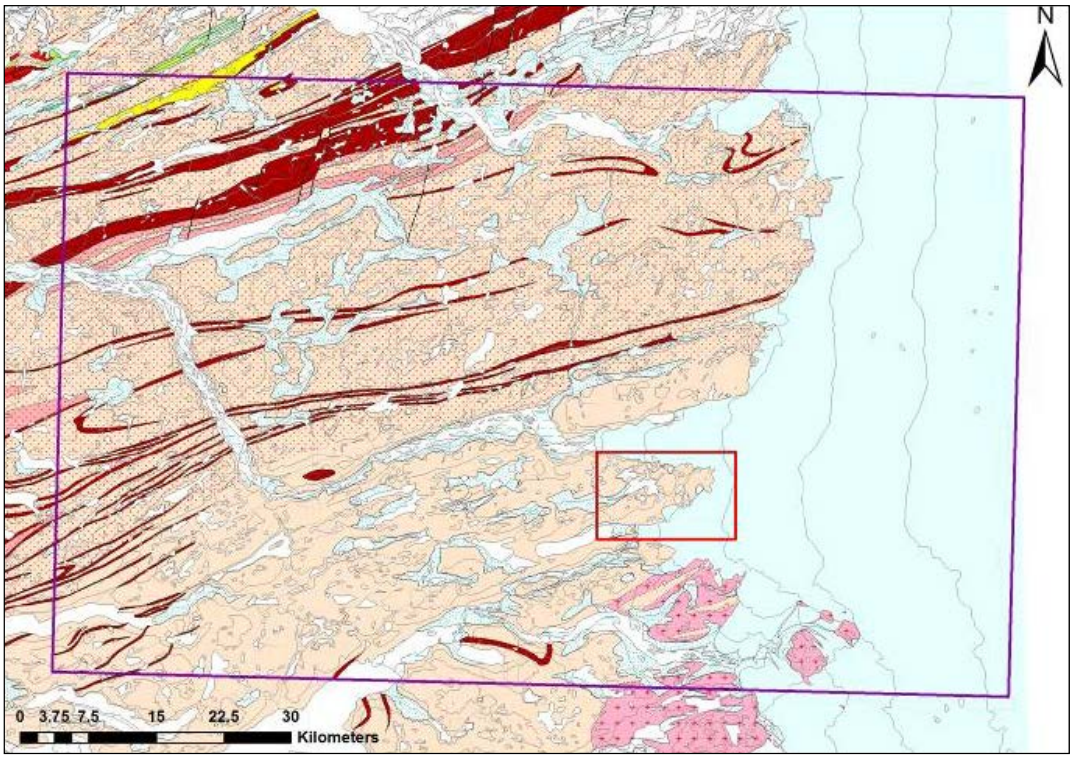


***Figure 1-3.*** *Map showing the regional model area of the "Geomodel" in lilac and the GAP site-scale area in red. The "Geomodel" (Engström et al. 2012) covers an area of approximately 70 km by 110 km. Geology is adapted from GEUS Geological map (Escher 1971).*

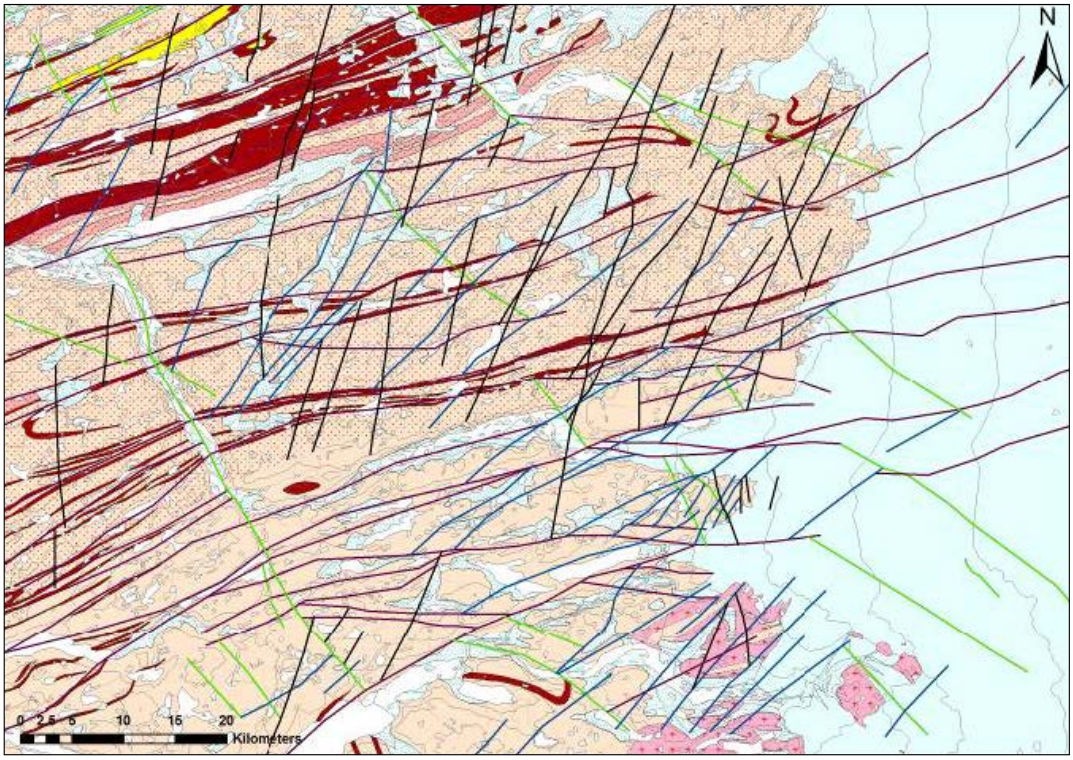


***Figure 1-4.*** *Map showing the final interpretation of Geomodel version 1 (Engström et al. 2012) with the four different types of deformation zones and faults: Type 1 = Lilac (oldest), Type 2 = Green, Type 3 = Blue and Type 4 = Black (youngest). Geology is adapted from GEUS Geological map (Escher 1971) (taken from Engström et al. 2012).*

The model contains four different vertical sets of potential deformation zones and faults (Figure 1-4). The Type 1 set (Lilac) trends ENE-WSW and cross cuts the entire area. The Type 2 set (Green) trends NW-SE, and the Type 3 set (Blue) trends NE-SW. The Type 2 and the Type 3 sets are both shorter than the Type 1 set, and might be a conjugate system with each other. The Type 4 set (Black) trends NNE-SSW and cross cuts all other types; hence it is the youngest of the four sets. Eighteen of 158 deformation zones/faults occur within the site-scale area shown in Figure 1-3, and most of them are supported by field observations.

Note that the "Geomodel" by Engström et al. (2012) used in the present model does not contain any horizontal or sub-horisontal deformation zones.

# 2 Hydrogeology under periglacial and glacial conditions

This section should be seen as a condensed literature review.

## 2.1 Glacial hydrogeology

The main characteristic of a periglacial landscape is the frozen ground. Permafrost is present if the ground temperature is at or below 0 °C for at least two consecutive years (e.g. French 1996). The greatest impact of permafrost on the subsurface hydrology is the phase change related to the freezing of groundwater, and permafrost is often imagined to create an almost impervious layer near the surface. This layer obviously decreases the potential groundwater recharge and discharge, highlighting the possibility of high groundwater pressures beneath the permafrost layer (e.g. Burt and Williams 1976, Kleinberg and Griffin 2005, Bense and Person 2008, Lemieux et al. 2008a, b, c among others).

The above definition of permafrost does not imply that the surface is completely frozen. Due to capillary forces, water does not freeze completely, and a thin film of liquid water covers the rock/soil grains even at low temperatures (e.g. Kane and Stein 1983). The unfrozen water content under permafrost conditions is sufficient to maintain the groundwater table at, or close to, the surface (Person et al. 2007). Physical permafrost models, which are based on the state equations for the phase change, suggest large variations in the unfrozen water content, and hence also in the hydraulic conductivity and transport properties, depending on the temperature and the geological material. Burt and Williams (1976) and Kleinberg and Griffin (2005) provide some information about the field permeability of soils as a function of the unfrozen water content, but on the whole, there are few field data reported in the literature. As a consequence, the choice of model parameters is often based on laboratory experiments (e.g. Williams and Smith 1989). Although there is consensus that the hydraulic conductivity of soils and rocks is greatly reduced by the freezing during permafrost conditions, there is, as it appears, neither a consensus on the magnitude of the reduction nor on how it should be modelled. Boulton and de Marsily (1997) concluded that the paucity of data to constrain the assumptions in glacial and permafrost modelling is evident. Thus, in the present context, the occurrence of taliks is considered to be an important feature (e.g. McEwan and de Marsily 1991, Boulton et al. 1993, Haldorsen and Heim 1999, Bosson et al. 2012, 2013).

A continental-scale ice sheet cycle implies that a very large region is covered by a thick ice sheet. The foremost part of a continental-scale ice sheet is generally believed to be underlain by permafrost to larger or smaller extent, whereas the thicker parts further in under the ice sheet are imagined to be underlain by unfrozen ground. This is due to accumulation of geothermal heat at the ice/bed interface, which will warm the ice to the melting point where the ice is sufficiently thick so that heat is conducted through the ice away from the interface at a slower rate than it arrives from below (e.g. Hughes 1998, Boulton et al. 1996, Boulton and de Marsily 1997, King-Clayton et al. 1995, Lemieux et al. 2008a).

During summer, surface melt water can gather in ponds or lakes on the surface of the ice sheet. From the surface, the surface melt water may reach the basal melt water through crevasses and/or moulins, at least in the ablation area of the ice sheet, i.e. in the region of the ice sheet where melt is sufficient to cause annual mass loss (Zwally et al. 2002, van der Veen 2007). Sub-glacial melt water is generated from geothermal heating of basal ice, sliding friction, and strain heating as the ice deforms, and this water will either flow towards the ice sheet margin through a transmissive layer[2] (e.g. Flowers and Clarke 2002, Breemer et al. 2002 among others) or recharge into the subsurface (e.g. Boulton et al. 1995, Piotrowski 1997a, b among others).

[2] A transmissive layer is in this report defined as a macro-scale thickness of liquid water existing at the interface between the ice sheet and its basal boundary. The layer may consist of channels, sheets, large cavities linked by small orifices, or some combination thereof, and may exhibit a wide range of flow conditions. The transmissive layer is an equivalent term for the ‘subglacial drainage system’.

Although widely recognised and commonly accepted, the concept of a transmissive layer between the ice and the geological substratum has been interpreted in very different ways in the past. Examples of studies that have considered different types of models under turbulent flow conditions are, e.g. Röthlisberger (1972) and Nye (1973). There are also examples of studies that have considered different types of models of "conduits" or "channels" under laminar flow conditions (e.g. Weertman 1972, Kamb 1987, Walder and Fowler 1994).

The abundance of eskers in the Fennoscandian Shield region demonstrates the frequency of major melt water tunnels during the retreat of the Weichselian ice sheet. The eskers occur at the ground surface on top of the crystalline bedrock, which reveals that it was here that the bulk of the melt water runoff took place. The high potential for discharging large amounts of melt water and glaciofluvial material would have resulted in a noticeable drawdown of the hydraulic head at the ice-subsurface interface along a melt water tunnel (Jansson et al. 2007, Boulton et al. 2007a).

The role of melt water tunnels for groundwater flow has been interpreted in different ways. Boulton et al. (1995) modelled groundwater flow in an approximately 1 500 km long transect extending from Norway to the Netherlands. A limited recharge of melt water into the subsurface was assumed, implying that the bulk of the melt water runoff at the ice-subsurface interface is not assumed to be a part of the groundwater flow on this scale. The limited recharge of melt water at the ice-subsurface interface is constrained by a criterion that the generated sub-glacial head at the ice-subsurface interface must be kept below the ice sheet elevation. Svensson (1999) and Jaquet and Siegel (2003) also used a prescribed recharge rate at the ice-subsurface interface. However, in contrast to Boulton et al. (1995), these authors used a 3D model domain with hydrogeological conditions typical of the Fennoscandian Shield. In particular, they included two extensive melt water tunnels of constant hydraulic conductivity and size in the flow model. The hydraulic conductivity of the tunnels is calibrated such that the prescribed recharge did not generate a sub-glacial head above the ice sheet elevation. The two tunnels are placed perpendicular to the ice sheet margin along the boundaries of the 250 km long model domain. This model is further elaborated by Jaquet and Siegel (2006), who included a stochastic component to represent heterogeneous hydraulic properties in the bedrock and in the Quaternary deposits between the two deterministically modelled melt water tunnels located at the edges of the model domain.

Boulton et al. (2007b) used a groundwater flow model to apply a theory that melt water tunnels, with dynamic (self-organising) geometrical and hydraulic properties, form at the ice-subsurface interface where groundwater recharge alone does not discharge the melt water flow without the generation of excess sub-glacial heads. The melt water tunnels are formed at locations near the ice sheet margin where high water flux produces sufficient heat to melt channels in the ice. This condition is likely to vary between seasons as water flux is modulated by surface melt and, as a consequence, the spacing between long-term stable melt water tunnels is likely to be determined by winter melt water flow rates if such stable tunnels exist.

In a regional context, the majority of these so-called transmissive layers are, however, not melt water tunnels or low-pressure channels. Further, as the subglacial drainage system is believed to evolve seasonally in response to melt input. These melt water tunnels form primary during summer and to collapse back into high-pressure distributed systems in winter. This indicates that most tunnel flow only occur during two or three months every year.

Meierbachtol et al. (2013) presented experimental results from Greenland suggesting that the subglacial system near the ice sheet margin (< 10 km) is a high-pressure system (e.g. linked-cavity, thin sheet flow, etc.) that locally may change into (or back from) a more connected low-pressure system (channel system) over the year. Further in beneath the ice, the transmissive layer seems to be stable in a high-pressure, more distributed, system simply since there is not enough energy to "grow" a stable conduit system beneath a thick ice. This finding is supported by the work of e.g. Werder et al. (2013) and Dow et al. (2015).

Based on hydraulic interference responses, Meierbachtol et al. (2013) conclude that the observed high-pressure system must be of a character resembling a linked-cavity system. Field observations on sub-glacial beds have indicated systems characterised by larger cavities caused by separation of the ice from the bed in the lee of small highs on the bed surface. The cavities seem to be linked by smaller orifices. Such observations (e.g. Walder and Hallet 1979) were later mimicked utilising a theory of a linked-cavity system (Kamb 1986). Figure 2-1 describes the conceptual model of Kamb (1986).

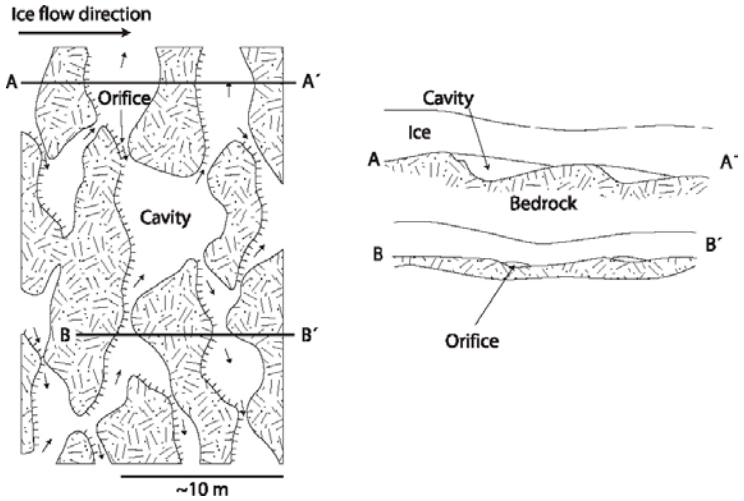


***Figure 2-1.*** *Conceptualisation of a linked cavity system (figure taken from Paterson 1994)*

In the linked-cavity system, the flow is controlled by the size of the orifice. This size in turn is dependent on the sub-glacial water pressure in relation to the ice load pressure. For high water pressures, e.g. floatation pressures, the size of the orifice becomes large and the linked-cavity system approaches a sheet-flow system with a significant and well-connected flow. This sheet flow may during certain conditions develop into temporary tunnels in order to discharge even more melt water.

Groundwater flow beneath a continental ice sheet is mainly due to two processes (e.g. Boulton et al. 1999, Clark et al. 2000, Douglas et al. 2000, Grasby et al. 2000, Ferguson et al. 2007, Person et al. 2007): (i) transient recharge and discharge conditions at the ice-subsurface interface, and (ii) contraction of the bedrock, which causes an expulsion of (or suction into) existing storage of groundwater in the fracture system.

The melt water is under ice sheet pressure and, where the hydraulic conductivity is sufficient, the melt water is driven into the subsurface. The hydraulic head required to keep a thick ice sheet floating on top of the sub-glacial melt water is typically 92 % of the ice sheet thickness (Paterson 1994). During its retreat, the height of the ice sheet profile is lower than during its advance (SKB 2010).

Lemieux et al. (2008a) modelled the dynamics of groundwater recharge and seepage over the Canadian Shield during the Wisconsinian glaciation (~ –120 ka to present). The authors concluded that, in the model, much of the infiltration of subglacial melt water occurred during ice sheet advance, whereas during ice sheet retreat, groundwater mainly exfiltrated at the surface, in both the subglacial and periglacial areas.

The deformation of the crust by the weight of the ice sheet implies that the Earth's surface elevation will be depressed underneath the ice sheet and raised beyond its margins. The full isostatic compensation of ice sheet loading is according to Marshall and Clark (2002) and Tarasov and Peltier (2004, 2007) 28 %, which implies that an ice sheet of a few kilometres thickness has a weight sufficient to depress the Earth's crust by about 1 km. Hence, it is also possible that the surface loading by glacial ice produces a mechanical deformation that increases subsurface pore pressure. By the same token, the increased load beneath a continental ice sheet could reduce the hydraulic conductivity through compression of pores and closure of fractures (Walsh and Avis 2010). Wang (2000) and Neuzil (2003) argued that the assumption of purely vertical strain below an ice sheet is a reasonable assumption in 2D and 3D flow regimes provided that only homogeneous and laterally extensive overburden changes occur. However, this assumption is not valid where vertical loads vary significantly within the model domain, as would occur at the margin of an advancing or retreating ice sheet margin. Consequently, the one-dimensional hydromechanical coupling suggested by Wang (2000) and Neuzil (2003) can only be viewed as an approximate solution, providing an estimate of how mechanical pressurisation of the subsurface under transient glacial loading might impact the flow field and the resulting solute transport conditions.

The assumption of Wang (2000) and Neuzil (2003) is invoked in the 3D studies by Lemieux et al. (2008a, b, c), Walsh and Avis (2010), Cohen et al. (2010) and Yin et al. (2013) to describe transient groundwater flow during the advance and retreat of a continental-scale ice sheet. In the safety assessment modelling performed by SKB (Vidstrand et al. 2010a, b), the only source of groundwater flow is the potential recharge at the ground surface in the proglacial area in front of the ice sheet margin, or at the ice sheet-subsurface interface. In lower strength rock of moderate to low permeability, water flow does not occur instantaneously when the prevailing pressure changes as in crystalline hard (high strength) rock with connected open fractures. That is, in lower strength rock of moderate to low permeability, an additional source of groundwater flow could be conceived to occur since the ice sheet loading may result in an expulsion of water due to a consolidation of the bedrock matrix as discussed above. In high strength, fractured (permeable) crystalline rock, such as the Fennoscandian Shield (Glamheden et al. 2007, Hakami et al. 2008, Mattila 2009) – and based on available knowledge most likely relevant for the GAP site bedrock – all pressure changes during a glacial cycle may be assumed to propagate instantaneously (Lund et al. 2009, Lönnqvist and Hökmark 2010, Hökmark et al. 2010, Vidstrand et al. 2013). Hence, neglecting the hydro-mechanical (HM) coupling is certainly valid for warm-based ice sheets, with sub-glacial water pressures yielding floatation, such as for the modelling cases and conditions assumed in the present modelling study. Ignoring HM-couplings will generally exaggerate the Darcy fluxes and the distortion of the salinity field at depth (e.g. Neuzil 2012).

## 2.2 Boundary conditions for groundwater flow models

It is from the above readily concluded that the top boundary conditions (hydraulic, thermal, as well as mechanical) are key to modelling groundwater flow beneath an ice sheet. Hydrogeological boundaries of a groundwater flow system are generally represented by the following three types of mathematical conditions (e.g. Anderson and Woessner 1992):

- Type 1. Specified pressure boundaries (Dirichlet conditions) for which pressure (or head) is given.
- Type 2. Specified flow boundaries (Neumann conditions) for which the flux across the boundary is given. A no-flow boundary condition is set by specifying the flux to be zero.
- Type 3. Pressure-dependent flow boundaries (Cauchy or mixed boundary conditions) for which flux across the boundary is calculated given a boundary pressure (or head) value. This type of boundary condition is sometimes called a mixed boundary condition because it relates boundary pressures to boundary flows. There are several types of pressure-dependent flow boundaries (see below).

Input data to the Type 1 (specified pressure) and Type 2 (specified flow) boundaries can either be derived from numerical ice sheet models, which generally assume that the bedrock is impermeable (e.g. Boulton and Payne 1993, Tarasov and Peltier 2004), or based on theoretical and/or empirical relationships for ice sheet thicknesses (pressure) or basal melt rates (flow) (e.g. Paterson 1994, Sugden and John 1976). These types of data have also been produced within the GAP and used by e.g Jaquet et al. (2012). The Type 3 (pressure-dependent flow) boundary condition normally implies some kind of penalty function that reduces flow if the simulated pressure exceeds a specified pressure limit, e.g. the flotation pressure.

Specified pressure beneath glacier ice has been used in various groundwater flow models (e.g. Piotrowski 1997a, b, Chan et al. 2005, Vidstrand et al. 2007, 2010a, b, 2013, 2014, Walsh and Avis 2010, Cohen et al. 2010, Normani and Sykes 2012). Piotrowski (1997a, b) assigned a specified pressure equal to 72 % of the ice sheet thickness beneath the ice sheet. This value was based on known consolidation rates and simulated ice thickness data in the clay sediments at the modelled site located in northern mainland Europe. Chan et al. (2005) modelled a site located in crystalline bedrock in inland Canada and assigned a specified pressure beneath the ice sheet equal to the flotation pressure, but also included cases with a large melt water tunnel of lower pressure. Part II of the present study uses a specified pressure boundary condition.

Applying a specified flow beneath a glacier ice has been attempted by e.g. Jaquet and Siegel (2006) and Piotrowski et al. (2009). Jaquet and Siegel (2006) tried to infiltrate the entire reconstructed discharge of glacial melt water (> 6 000 mm/year), derived from both surface and basal melting, for a modelled site located in crystalline bedrock in south-eastern Sweden. Jaquet and Siegel (2006) concluded that even with the incorporation of an extensive layer of Quaternary deposits and a sub-glacial tunnel model (consisting of temporally static elongated high-permeable pathways representing melt water tunnels) on top of the bedrock, the assigned specified flux had to be significantly reduced (down to below 200 mm/year) in order to keep the pressure below the ice sheet flotation pressure. Piotrowski et al. (2009) analysed a substantially more modest melt rate, from basal melting only (36 mm/year), for a modelled site located in northern mainland Europe. Although the entire model was made up of unconsolidated sediments with significant transmissivity values, the authors concluded that the specified flux of melt water had to be reduced by 70 % in order to keep the pressure below the ice sheet flotation pressure.

Examples of studies where pressure-dependent flow boundaries have been used are e.g. Boulton et al. (1995), Svensson (1996), Jaquet and Siegel (2006) and Lemieux et al. (2008a, b, c), Svensson (1996) used a classic Cauchy condition where the specified flux (representing basal melt rate only) caused a pressure exceeding the flotation pressure; the value was re-calculated using a specified pressure equalling the flotation pressure. Jaquet and Siegel (2006) simply reduced the specified flux until the resulting pressure was below the flotation pressure. Lemieux et al. (2008a, b, c) assigned a specified flux based on simulated basal melt rates taken from Tarasov and Peltier (2004). However, where the resulting pressure exceeded the flotation pressure, the specified flux was shifted to a specified pressure that equated 92 % of the simulated ice sheet thickness.

An alternative to a penalty function used in mixed boundary conditions is to change the associated geological conceptual model and to modify the initially assigned hydraulic conductivity values. Examples of studies where this latter approach have been used are e.g. Flowers and Clarke (2002), Breemer et al. (2002), Moeller et al. (2007), Carlson et al. (2007), and Bense and Person (2008). These types of models are generally very successful in creating a good representation of the system, hence clearly highlighting the importance of the use of a good conceptual model of the interface between the ice sheet and the subsurface. This latter approach is the main approach in Part I of the present modelling study.

# 3 Concepts and methodology

The simulations have been conducted with the DarcyTools code (Svensson et al. 2010), which is a finite volume code that represents discrete features such as fractures and fracture zones by employing volumetric up-scaling. This implies that an equivalent continuous porous medium (ECPM) approach is invoked; see e.g. Svensson (2001a, b) for details. In this approach, each numerical cell has a permeability value based on the volumetric amount of fractures and deformation zones belonging to a cell. Fractures and deformation zones have individual transmissivity values, whereas the rock mass has a low, background permeability value.

To account for phase changes of water when the temperature drops below freezing, the mass conservation equation, mass fraction transport equations, and the heat transport equation all have to be modified. In addition, properties such as permeability and thermal conductivity need to be modified to account for freezing.

Frozen ground is, in reality, a four-component system consisting of bedrock, frozen fluid (ice), unfrozen fluid (e.g. water) and gases (e.g. air). Assuming that the pore space of the groundwater system is unchanged and filled with either ice or water, i.e. ignoring the possibility of a gaseous phase and simply adding the ice phase to a single fluid phase, a simplified ice content function ε is employed (Mottaghy and Rath 2006):

$$\phi_i = \varepsilon\,\phi$$
$$\phi_f = (1-\varepsilon)\,\phi \qquad \text{(Eq 3-1)}$$

where $\phi$ is the total kinematic porosity [–], $\phi_i$ is the part of the kinematic porosity filled with ice, $\phi_f$ the part filled with water, and $\varepsilon$ represents the ice content function. $\varepsilon$ is generally assumed a continuous function of temperature and is given by Lunardini (1988) and Mottaghy and Rath (2006):

$$\varepsilon = \varepsilon_{\max}\left(1-\exp(-\beta_\theta)\right)$$
$$\beta_\theta = \left(\frac{\min\{\theta,\theta_L\}-\theta_L}{w}\right)^2 \qquad \text{(Eq 3-2)}$$

where $\varepsilon_{max}$is the maximum value (generally assumed to be 1), $\theta_L$ is the thawing temperature, and $w$ is a thawing interval which has to be adapted to the simulated ground conditions (material). The thawing temperature is dependent on both the salinity and the pressure at the calculation point. In this study, however, these dependencies are ignored and the thawing temperature is fixed at zero degrees C; this since the melting process of the ground in itself has limited importance for groundwater flow.

The introduction of an ice phase dependent on the temperature links the conservation equations which become non-linear. When the densities of the solid (ice) and fluid phase differ, there is a motion of the fluid due to changes in volumes. Incorporating these effects yields a mass conservation equation as follows:

$$\frac{\partial \rho_f \phi}{\partial t} + \frac{\partial(\rho_i-\rho_f)\varepsilon\phi}{\partial t} + \frac{\partial}{\partial x}(\rho_f u) + \frac{\partial}{\partial y}(\rho_f v) + \frac{\partial}{\partial x}(\rho_f w) = Q \qquad \text{(Eq 3-3)}$$

where $\rho_f$ is fluid density [$ML^{-3}$], $\rho_i$ is ice density [$ML^{-3}$], $t$ is time [T] ($u$, $v$, $w$) are the directional components of the volumetric (Darcy) flux $\mathbf{q}$ [$LT^{-1}$] at the location ($x$, $y$, $z$) [L,L,L] in a Cartesian coordinate system, and $Q$ is a source/sink term per unit volume of fluid mass [$ML^{-3}T^{-1}$]. The mass conservation equation is turned into a pressure equation by invoking Darcy's law:

$$u = -\frac{k_x}{\mu}\frac{\partial P}{\partial x}$$
$$v = -\frac{k_y}{\mu}\frac{\partial P}{\partial y} \qquad \text{(Eq 3-4)}$$
$$w = -\frac{k_z}{\mu}\frac{\partial P}{\partial z} - \frac{k_z}{\mu}\left(\rho_f - \rho_0\right)g$$

where $k_x$, $k_y$ and $k_z$ are the orthogonal components of the permeability tensor parallel to the Cartesian coordinate system [$L^2$], $\mu$ is the fluid dynamic viscosity [$ML^{-1}T^{-1}$], $g$ is the acceleration due to gravity [$LT^{-2}$], $\rho_0$ is a reference fluid density [$ML^{-3}$], and $P$ is the dynamic fluid pressure [$ML^{-1}T^{-2}$] at the location ($x$, $y$, $z$):

$$P = p + \rho_0 g\, z \qquad \text{(Eq 3-5)}$$

where $p$ is the gauge pressure [$ML^{-1}T^{-2}$] and $\rho_0 g z$ is the hydrostatic pressure, $P_0$. The dynamic fluid pressure, $P$, is used for numerical reasons, i.e. in order to avoid storing large numbers in the computations.

The hydraulic conductivity $K$ [$LT^{-1}$] is related to the permeability $k$ through the relation:

$$K = \frac{\rho_f\, g}{\mu}k \qquad \text{(Eq 3-6)}$$

Although density effects are ignored in the present work, the following section describes how DarcyTools handles variable-density flow at isothermal conditions, which can be assumed valid at repository depth.

The parameters $\rho_f$ and $\mu$ are given by the following state laws:

$$\rho_f = \rho_0\left[1 + \alpha C\right] \qquad \text{(Eq 3-7)}$$

$$\mu = \mu_0 \qquad \text{(Eq 3-8)}$$

where $\alpha$ and $\mu_0$ are constants and $C$ represents the salinity (mass fraction) [-]:

$$C = TDS / \rho_f \qquad \text{(Eq 3-9)}$$

where TDS is the abbreviation of Total Dissolved Solids [$ML^{-3}$]. The migration of salt is modelled in terms of advection and diffusion processes in the mobile pore system and as a diffusion process in an immobile (rock matrix) pore system simulated by the multi-rate methodology (Haggerty and Gorelick 1995). The advection-diffusion equation for the mobile pore system is modelled according to the following equation:

$$\begin{aligned}\rho\phi\frac{\partial C}{\partial t} &+ \frac{\partial}{\partial x}\left(\rho_f u C - \rho_f \gamma D_x \frac{\partial C}{\partial x}\right)\\ &+ \frac{\partial}{\partial y}\left(\rho_f v C - \rho_f \gamma D_y \frac{\partial C}{\partial y}\right)\\ &+ \frac{\partial}{\partial z}\left(\rho_f w C - \rho_f \gamma D_z \frac{\partial C}{\partial z}\right) = QC + Q_C\end{aligned} \qquad \text{(Eq 3-10)}$$

with:

$$\rho = \rho_f + (\rho_i - \rho_f)\varepsilon \qquad \text{(Eq 3-11)}$$

where $\varepsilon$ is given by Eq 3-1, $D_x$, $D_y$ and $D_z$ are the orthogonal components of the diffusion tensor parallel to the Cartesian coordinate system [$L^2T^{-1}$], $QC$ and $Q_c$ are source/sink terms per unit

volume of fluid mass [$ML^{-3}T^{-1}$], where $Q_c$ represents the diffusive exchange of salt per unit volume of fluid mass between the mobile and immobile pore volumes [$ML^{-3}T^{-1}$] and where C is always the computed value, and $\gamma$ is a dimensionless coefficient that describes the dependency of the kinematic porosity of the mobile pore system on the dynamic pressure:

$$\phi = \phi_0 \, \gamma \tag{Eq 3-12}$$

$$\gamma = 1 + \frac{S_s}{\phi_0} \frac{\left(P - P_0\right)}{\rho_f g} \tag{Eq 3-13}$$

where $S_s$ is the specific storage, including all compressibility effects of the conductive pore system [$L^{-1}$] see e.g. de Marsily (1986).

The physical interpretation of the multi-rate diffusion model of Haggerty and Gorelick (1995) used is, in principle, to specify the penetration depth, $L_i$ [L], of each exchange rate coefficient, $\alpha_i$ [$T^{-1}$], as:

$$L_i = 2\sqrt{\left(\frac{D_e}{\phi_m \alpha_i}\right)} \tag{Eq 3-14}$$

where $D_e$ [$L^2T^{-1}$] is an effective diffusion coefficient and $\phi_m$ is the matrix porosity [-].

The penetration depth of the remotest diffusive exchange rate is estimated by inserting the minimum exchange rate coefficient into Eq 3-14. The value of the matrix porosity is estimated from the following relationship:

$$\phi_m = \beta \, \phi \tag{Eq 3-15}$$

where $\beta$ [-] is the ratio between the diffusive and advective pore spaces and $\phi$ is the grid cell kinematic porosity [-].

It is noted that for the modelled domain size, the salinity is assumed constant and practically zero (i.e. fresh water conditions prevail) and hence the salt related equations are not solved.

Using Eq 3-1, the heat conservation equation may be written as:

$$\begin{aligned}
&\rho\phi \frac{\partial c_{pf}\theta}{\partial t} + \frac{\partial (1-\phi) c \, \theta}{\partial t} + \frac{\partial \phi c_i \theta}{\partial t} - \rho_i L \frac{\partial \varepsilon}{\partial \theta} \phi \frac{\partial \theta}{\partial t} \\
&+ \frac{\partial}{\partial x}\left(\rho_f u c_{pf}\theta - \lambda_x \frac{\partial \theta}{\partial x}\right) \\
&+ \frac{\partial}{\partial y}\left(\rho_f v c_{pf}\theta - \lambda_y \frac{\partial \theta}{\partial y}\right) \\
&+ \frac{\partial}{\partial z}\left(\rho_f w c_{pf}\theta - \lambda_z \frac{\partial \theta}{\partial z}\right) = \left(\frac{\partial \rho_f u}{\partial x} + \frac{\partial \rho_f v}{\partial y} + \frac{\partial \rho_f w}{\partial z}\right) c_{pf}\theta + Q_T
\end{aligned} \tag{Eq 3-16}$$

with:

$$c_i = \rho_i (c_{pi} - c_{pf}) \varepsilon \tag{Eq 3-17}$$

where ε is given by Eq 3-1, $\rho$ is described by Eq 3-11, $\theta$ is the temperature [K], $c_{pf}$ is the specific heat capacity of the fluid and $c_{pi}$ is the specific heat capacity of ice [$L^2T^{-2}K^{-1}$] (or [J/(kg K)]), $c$ is the specific heat capacity of the ground [$L^2T^{-2}K^{-1}$] (or [J/(kg K)]), $L$ is the specific latent heat [$L^2T^{-2}$(or J/kg)], and $\lambda_x$, $\lambda_y$, and $\lambda_z$ are the directional components of the equivalent (i.e. matrix with fluid) thermal conductivity tensor [$MLT^{-3}K^{-1}$] (or [W/(m K)]). $Q_T$ represents a sink/source term [$ML^{-1}T^{-3}$] ([or $W/m^3$]). Eq 3-17 is introduced since it corresponds to the numerical implementation in DarcyTools. One should note that $C_i$ is not the thermal capacity of ice, but a numerical quantity.

The individual phases are assumed randomly distributed within a unit volume and, hence, the thermal conductivity is computed as a mean square root weighting of the three phases' (matrix, fluid, ice) individual thermal conductivities. However, as the thermal conductivity of the matrix is not directly used, but instead the equivalent thermal conductivity of the unfrozen material, the thermal conductivity of frozen ground is computed as (Mottaghy and Rath 2006):

$$\lambda = (\sqrt{\lambda_{ref}} + (\sqrt{\lambda_i} - \sqrt{\lambda_f})\varepsilon\phi)^2 \qquad \text{(Eq 3-18)}$$

where $\lambda_{ref}$ is the equivalent thermal conductivity of the saturated matrix, $\lambda_i$ is the ice thermal conductivity and $\lambda_f$ is the thermal conductivity of the fluid, all with units of [$MLT^{-3}K^{-1}$] (or [W/(m K)]).

Using a thawing interval (*w,* Eq 3-2) close to 0.1 provides good similarity between different laboratory data (e.g. Anderson and Tice 1973) for temperatures close to the freezing point. In the present study, the permeability is reduced by a power function of the unfrozen water content:

$$k = \alpha k_{ref} \qquad \text{(Eq 3-19)}$$

with:

$$\alpha = \max\left(\alpha_{\min}, (1-\varepsilon)^a\right) \qquad \text{(Eq 3-20)}$$

where the subscript '$_{ref}$' indicates the reference values associated with unfrozen conditions. Different combinations of the parameters, $w$ and $\alpha$, makes it possible to mimic experimental results reported for different ground conditions.

# 4 Hydrogeological model of the GAP study area

The sections below focus on the results that relate to the original objectives of the study. These results mainly originate from Part I of the study. However, results from Part II of the study are presented in order to illustrate what further investigations may be deemed relevant in order to achieve a better process and site understanding. Furthermore, the Part II results are also used for drawing conclusions at the end of the report.

## 4.1 Computational code

The groundwater flow modelling presented here uses version 3.3 (Part I) and 3.4 (Part II) of the DarcyTools computational code. These versions of DarcyTools contain an algorithm that is used to simulate changes in permeability due to freezing and thawing (Vidstrand et al. 2014). Changes in groundwater salinity due to freezing and thawing are not considered; this is generally considered a valid assumption in areas of mainly fresh water conditions such as in the GAP study area.

## 4.2 Part I data

In the Part I study, the input data are based on:

- DEM: a 5 km gridded surface, bed and thickness values. Data taken from Bamber 1993–1999, and available at the "National Snow and Ice Data Centre", http://nsidc.org/data/nsidc-0092.html.
- Coordinates: the coordinate system of the Bamber data set was used.
- Fracture data: Stochastic data generated based on Forsmark data for the FFM02 fracture domain (Follin et al. 2011).[3]
- Ice sheet margin and talik locations: Digitalised data from a Landsat satellite image from August 23, 2000. The talik elevations were obtained from the ASTER GDEM version 1 (https://asterweb.jpl.nasa.gov/gdem.asp).

## 4.3 Part I data processing

The reported data in this section refer to data analysed and used in the first part of the study (Part I).

Despite the generic character of the reported part I, the study is based on site-specific information from the GAP study area. Figure 4-1 illustrates the model domain in relation to Greenland continental scale, and specifically in comparison to the model domain used by Jaquet et al. (2010).

Figure 4-2 shows the discretization of the DEM available during Part I of the present study. Figure 4-3 illustrates the steps adopted in a refining of the DEM from the 5 km scale down to a 50 m scale. The refinement was conducted using the software Surfer and its predefined set-up of the Surfer kriging routine. The routine creates a smooth surface while honouring values at positions where data exist in the original DEM.

Figure 4-4 shows in orange lines the deformation zone model used to represent fractures. The deformation zone model is primarily stochastic and incorporates only a few site-specific data. Knowledge on existing deformation zones beneath the ice sheet is lacking. The black lines illustrate fracture sets that have been generated based on Swedish site data from the Forsmark site (the FFM02 fracture domain, Follin 2008).

[3] At the initiation of part I, little was known of the geological settings at the GAP site. The applied properties were based on Forsmark characteristics due to its usage within the Swedish programme for final disposal of spent nuclear fuel.

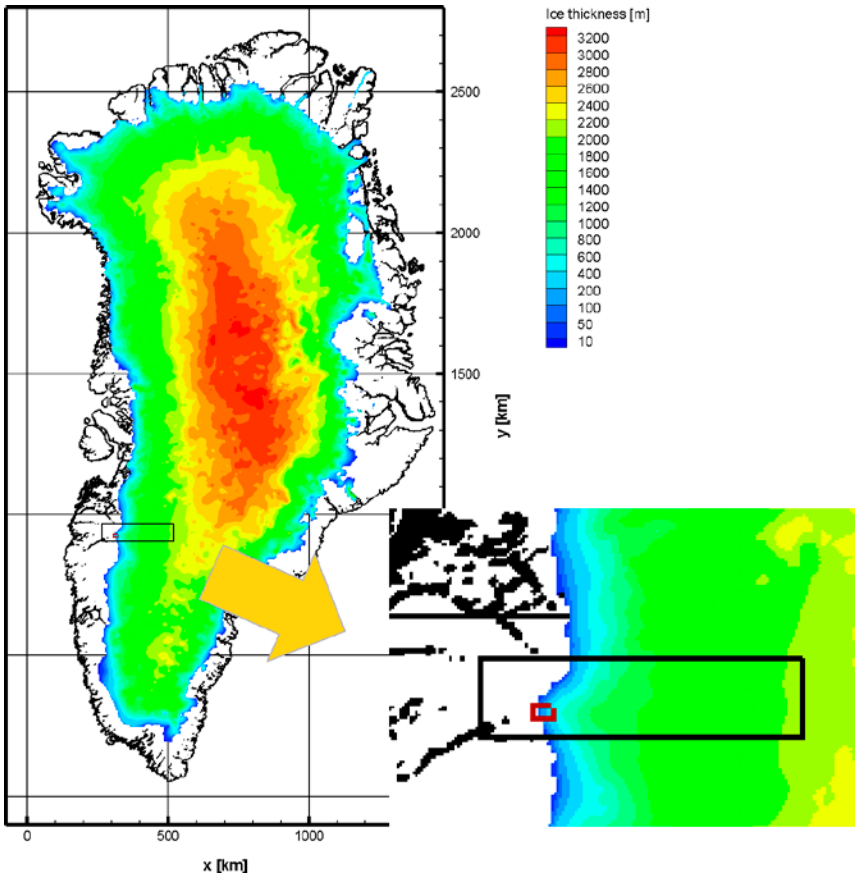


***Figure 4-1.*** *Illustration of model domains used by SKB and Posiva funded modelling studies. The larger black rectangle shows the modelling domain used by Jaquet et al. (2010), and the red smaller rectangle shows the model domain used in Part I of the present report.*

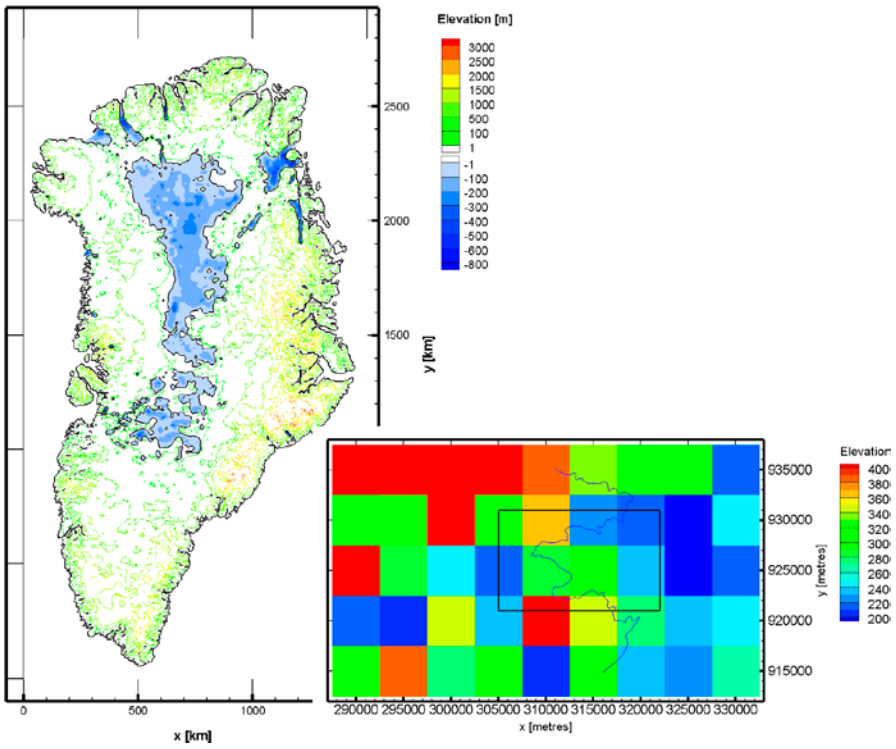


***Figure 4-2.*** *Illustration of the DEM (Bamber 1993–1999) available for the model domain used. The domain is shown with the black rectangle and incorporates twelve DEM data points. The thin blue line indicates the assumed location of the ice sheet margin.*

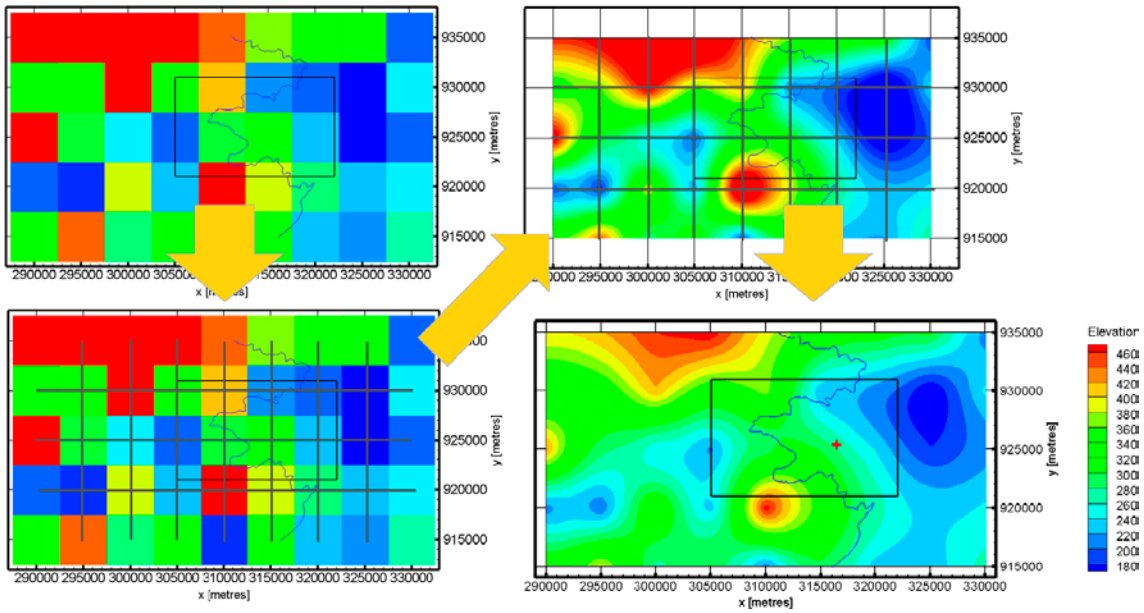


***Figure 4-3.*** *Illustration of the steps from the original DEM (Bamber 1993–1999) to the refined DEM used for top boundary specifications. The refinement was conducted using the software Surfer and its predefined set-up of the Surfer kriging routine. The routine creates a smooth surface while honouring values at positions where data exist in the original DEM. The thin blue line indicates the assumed location of the ice sheet margin.*

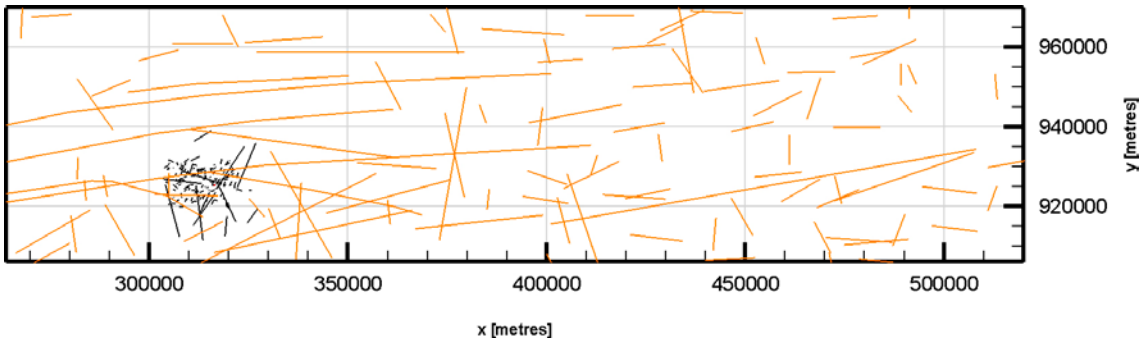


***Figure 4-4.*** *Illustration of the generic (stochastic) deformation zone model (orange). The black lines show the stochastic fractures generated based on Forsmark FFM02 statistics within a sub-volume that incorporates the used model domain.*

Figure 4-5 shows two cross-sections of the model grid in DarcyTools. The grid has been developed using the routine that removes cells deemed to be of no importance. In this case, cells with no fractures are removed. The routine is built on the idea of a successive refinement of cell sizes; the end product is close to a classical DFN model while still maintaining the merits of a finite volume porous medium code.

Figure 4-6 shows a horizontal cross-section and the grid representation of the generated fractures. The cell removal routine allows DarcyTools to create a model with high resolution and discrete flow paths; this may be essential if detailed information is demanded.

The discrete fracture system at depth is connected to the surface through a thin, approximate two metres thick geological layer (see Figure 4-7) of successively changing conductivity. The majority of this two metre thick layer is representing the uppermost part of the bedrock with typically increased fracturing.

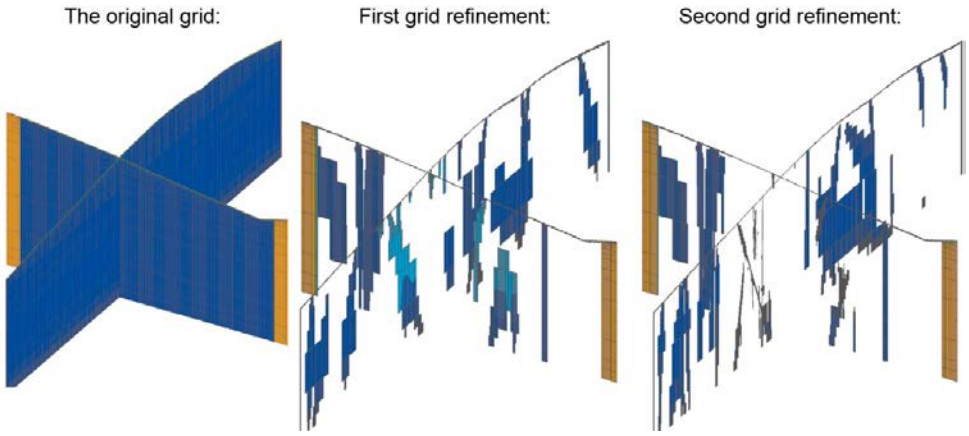


***Figure 4-5.*** *Illustration of the grid used in DarcyTools for two cross-sections. The figure shows the development of the grid from the starting point with a complete grid, to a developed grid where cells without fractures are removed. The third-step grid is used in the simulations reported here.*

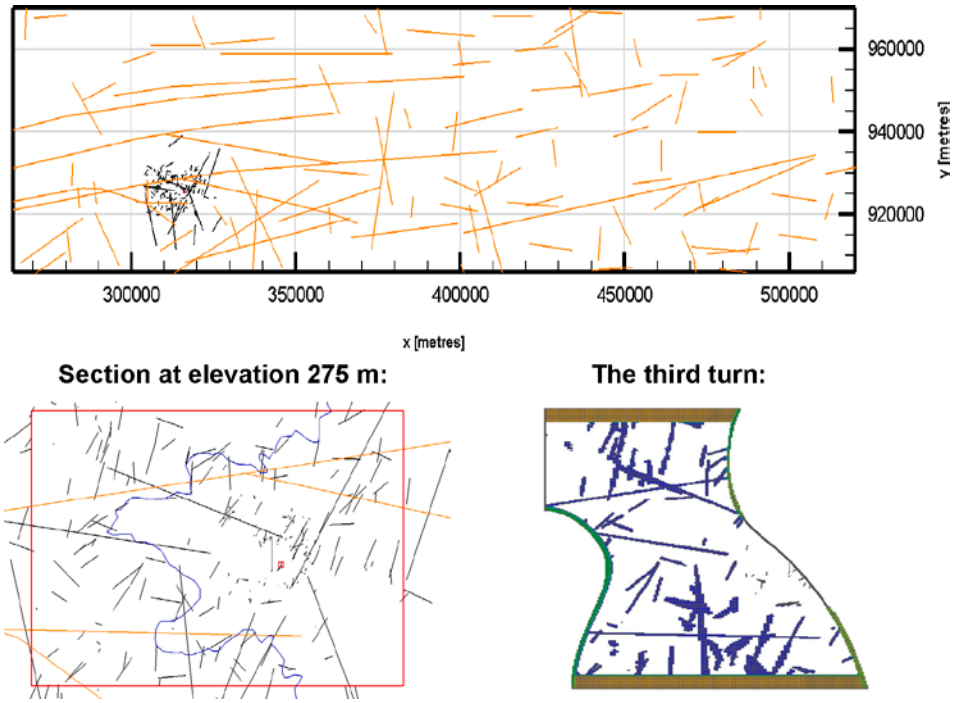


***Figure 4-6.*** *Illustration of the fractures from the large scale down to the model domain used (red rectangle in lower left). The lower left figure represents the generated fractures (shown as traces at elevation 275 m) and the lower right figure the final grid at the same elevation (275m). The ice sheet margin is shown in the lower left figure as a blue line. The generated fractures are clearly visible in the grid.*

The upper centimetres of this geological layer have a hydraulic conductivity around 1 m/s, which represents the subglacial transmissive layer, while the fracture network yields conductivity values at depth around 8–12 orders of magnitude lower. At the connection at a depth of two metres, the conductivity is around $1 \times 10^{-6}$ m/s. A description of the uppermost centimetres of the continuous top layer is provided later in more detail. This is done for a small part, the "detailed area"; however, the main parts of the surface layer have been assigned a homogeneous transmissivity value. Typically this also means a constant hydraulic conductivity, but in areas with for instance "large" changes in elevation, the unstructured grid may generate different cell thicknesses and hence small differences in hydraulic conductivities may occur. The glacial forefield is represented as a till material, but the transmissive layer between the ice and the geological substratum has a high hydraulic conductivity as described above (see Figure 4-8).

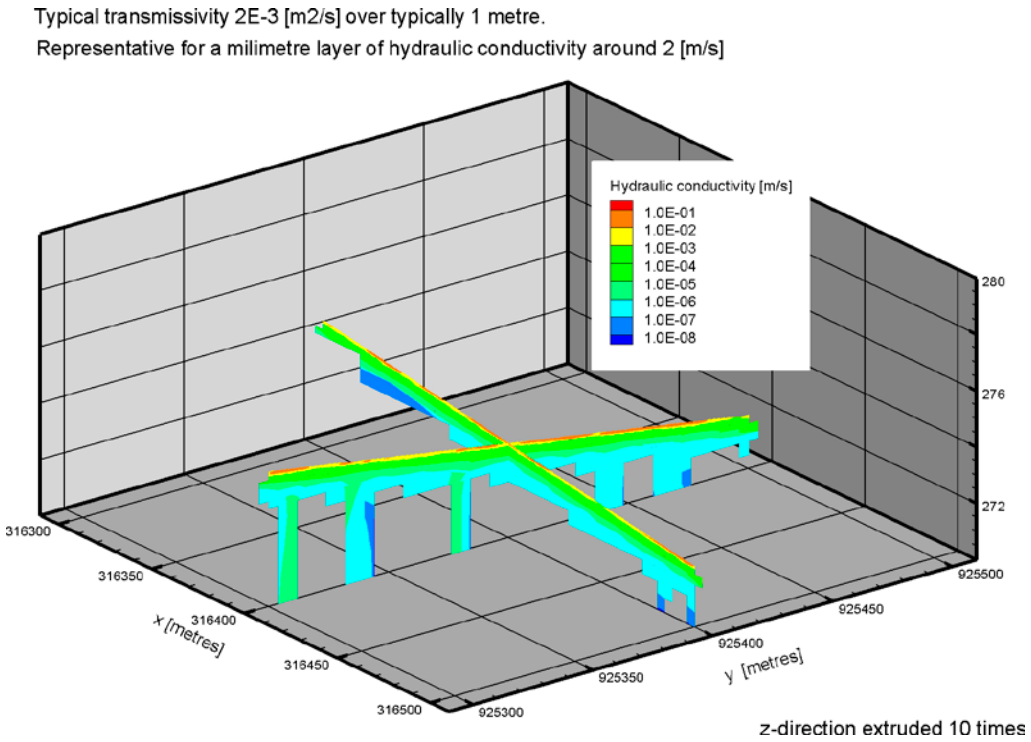


***Figure 4-7.*** *Illustration of the surface and how it connects with the "discrete" system at depth.*

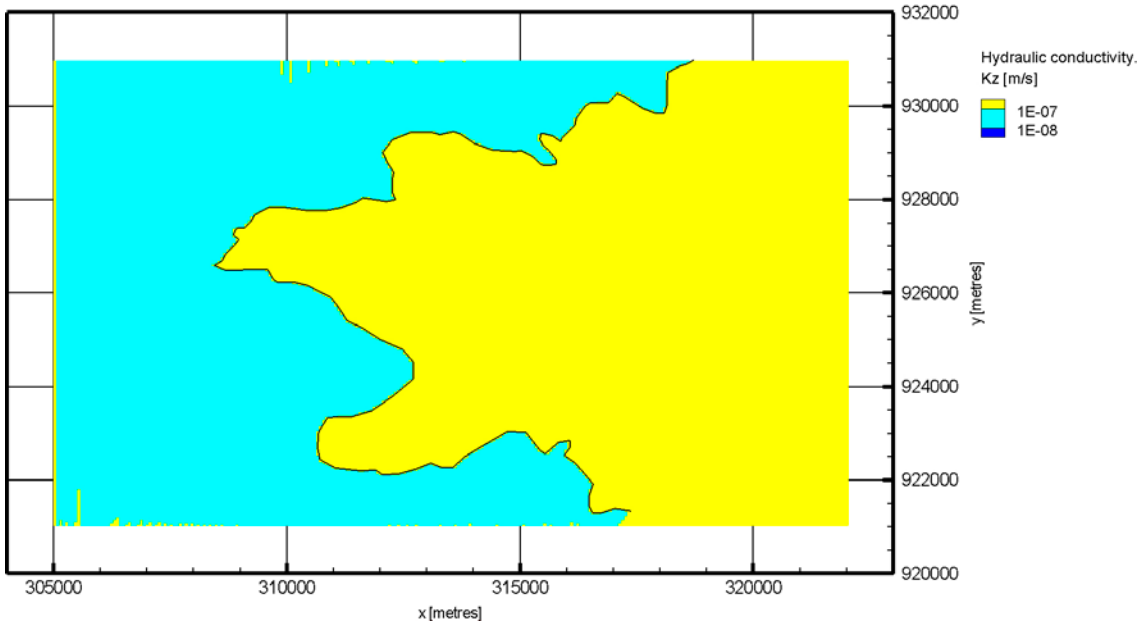


***Figure 4-8.*** *Illustration of vertical hydraulic conductivity. The ice sheet is the yellow region in the right side of the figure.*

Figure 4-9 shows two generic surfaces of the size 200 by 200 metres created with two different stochastic methods. In this study, an assessment of two statistical methods for creating a transmissive layer beneath the ice, but above the geological substratum, has been made. The transmissive layer is for modelling purposes here represented by a distribution of hydraulic conductivity value with an assumed geometrical mean value of 1 m/s.

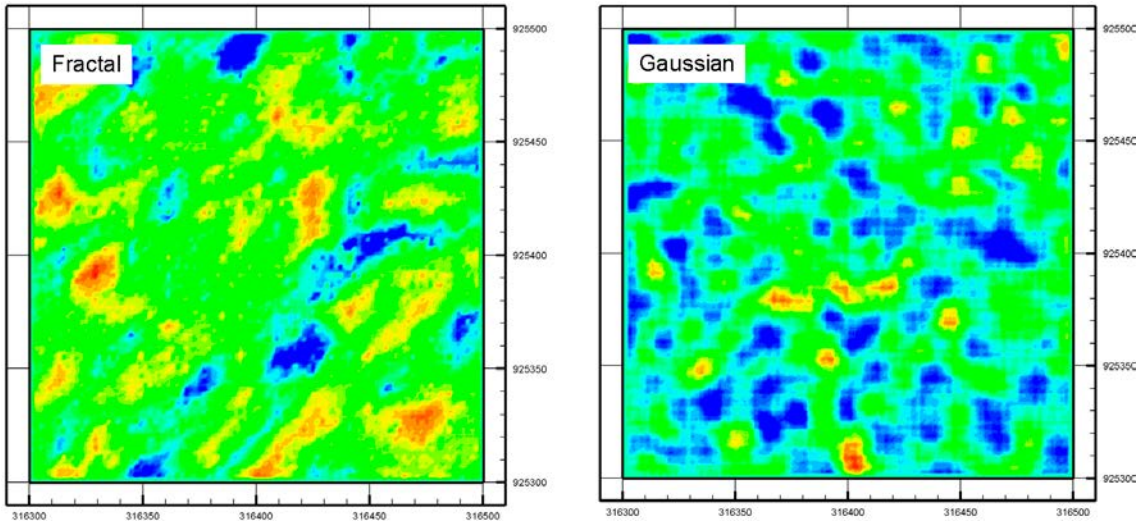


***Figure 4-9.*** *Illustration of two generic surfaces of size 200 by 200 metres, created with a Fractal stochastic method (left) and a Gaussian stochastic method (right). Colours indicate the flow capacity of a subglacial transmissive layer, where red indicate a high and blue a low flow capacity.*

The conceptual idea behind the stochastic surface and its variation is primarily based on the author's view of a linked cavity system. It should be noted that little is known about the specific characteristics of the linked cavity system, and there are likely site specific differences. The system is likely to be dependent on the bedrock roughness, and the ice sliding speed and local water pressure which influence the opening of cavities.

In the literature, notions of reasonable sizes of wet areas are stated to be approximately 10 metres and that such 10 metre size "pools" of water are connected with small "straw-like" pipes and that each "pool" is surrounded by ice in direct contact with bedrock interfaces having no permeability (e.g. Paterson 1994), i.e. areas with no available water.

The Gaussian surface of Figure 4-9 is reproduced in Figure 4-10 with one change. All parts of the stochastic surface are assigned values according to a hydraulic conductivity distribution, but hydraulic conductivity values below a certain threshold (0.1) are lowered significantly (down to $1 \times 10^{-6}$); this "new" system is thereafter introduced as a sub-part within the larger-scale model and the flow in this detailed sub-model is investigated (see Figure 4-11).

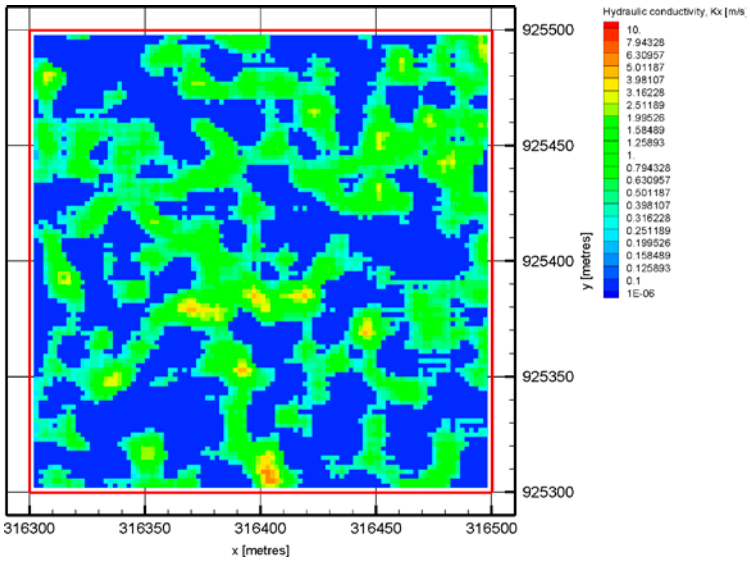


***Figure 4-10.*** *The Gaussian surface manipulated so that all values below a certain threshold are lowered significantly into a homogeneous and low conductive value. The green to red areas indicate the connected system of linked cavities.*

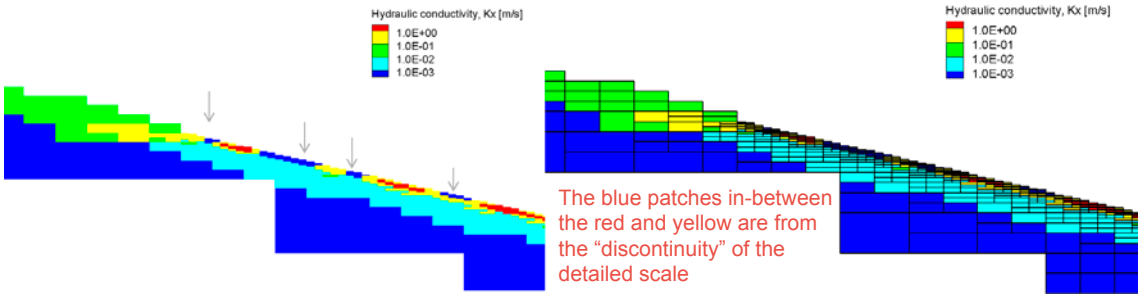


***Figure 4-11.*** *Illustration of the top layer of the model including the detailed area and the patchy behaviour of the hydraulic conductivity. In the right panel, the gridding is illustrated. The z direction of the detailed area is only on the 1 centimetre scale.*

## 4.4 Part I boundary conditions

Note that the top boundary condition for the part of the modelling domain that is below the ice sheet is assigned a flux boundary condition. Specifically, a high recharge value is assigned. However, in areas where a lower conductivity is apparent, the top boundary condition is set as no flow.

Figure 4-12 shows the detailed area for which results will be presented in the following sections. In the figures, all parts of the surface with lower conductivity ($< 1 \times 10^{-6}$ m/s) will be blanked out in order to highlight the channel-like flow behaviour of a linked cavity system.

The boundary conditions of the model are illustrated in Figure 4-13. The bottom boundary is a no-flow boundary. The lateral boundaries are no-flow boundaries except for the upstream boundary which is a specified pressure boundary (upstream herein also coincide with the position of the model domain that is furthest away from the ice sheet margin). In the illustrating figures, the specified pressure is set to 70 % of the ice thickness; i.e. 70 % of the difference between the refined DEM of the ice surface elevation and the refined DEM of the ground surface elevation. Different specified pressures were investigated but were found to yield no effect within the sub-volume of interest. The refinement of both DEMs is done identically and is presented earlier see Section 4.2.

In front of the ice sheet, the top boundary is a specified pressure boundary. The lateral boundary variants are either zero flow or a specified higher value, as discussed above.

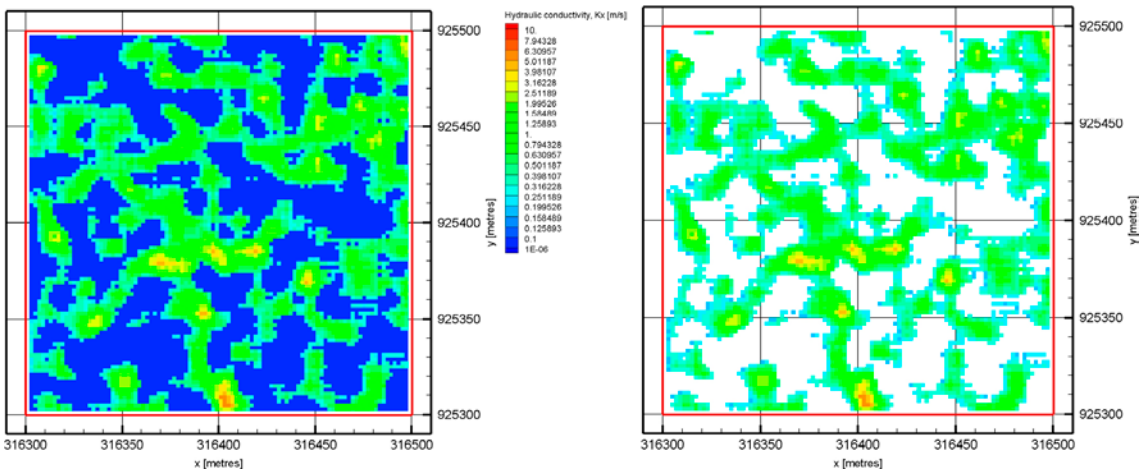


***Figure 4-12.*** *Illustration of how the simulated results will be presented in the following sections. The Gaussian surface manipulated so that all values below a certain threshold are lowered significantly into a homogeneous and low conductive value (dark blue) and these areas are later removed as is shown right.*

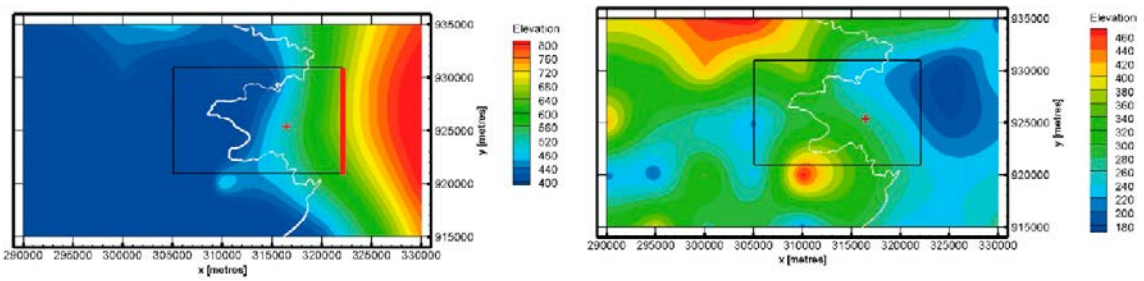


***Figure 4-13.*** *Illustration of how boundary conditions are applied. Left: black rectangle shows model domain; red line indicates the lateral boundary with a specified head boundary applied as 70 % of the ice sheet thickness. All other lateral boundaries, as well as the bottom boundary, are set as no-flow boundaries. Right: The surface elevation. In front of the ice sheet, the surface elevation is used to specify a pressure. Below the ice sheet, the boundary condition is a flux at the top of the surface cells. The red marker indicates the focused area. Thin white line indicates the assumed position of the ice margin.*

## 4.5 Part I results

Figure 4-14 to Figure 4-21 present the main findings of Part I.

In summary, a small sub-area of the entire model was investigated (see e.g. Figure 4-13). This sub-area has a fine discretization of a transmissive surface layer mimicking a linked-cavity system. Different characteristics of this transmissive layer were analysed.

Figure 4-14 illustrates the conceptualized linked-cavity system with fully developed contacts between cavities. The hydraulic conductivity distribution is based on a Gaussian distribution where the high transmissive parts are connected. This is a plausible and relatively realistic description of

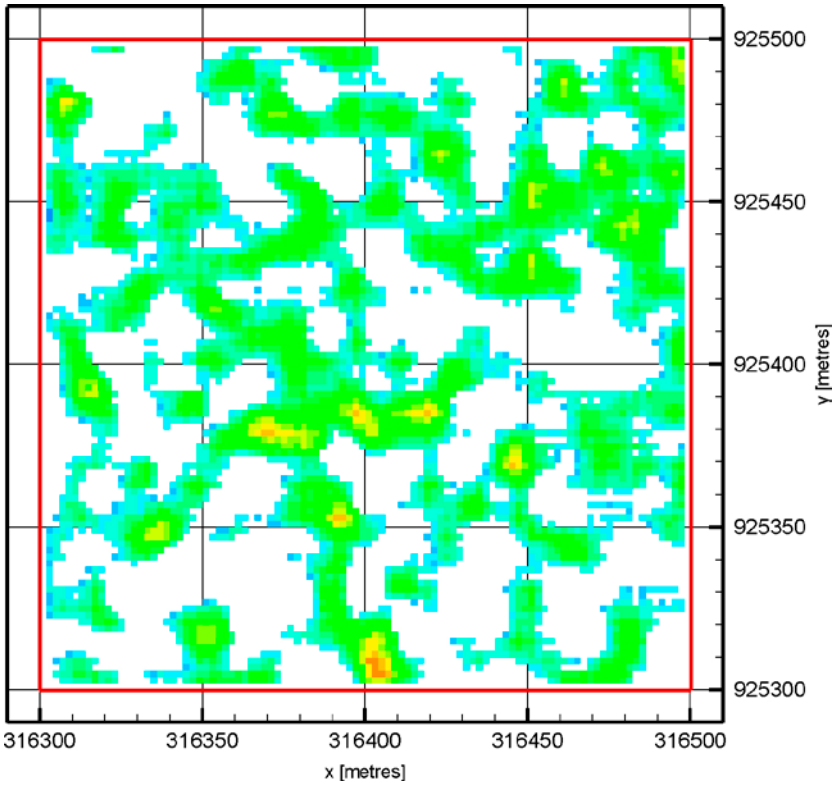


***Figure 4-14.*** *Gaussian multivariate distribution of hydraulic conductivity with a correlation length of 8 m. The parts of the generated surface with hydraulic conductivity larger than 0.1 m/s were saved and used for detailed groundwater flow analyses. In white areas, a no-flow top boundary is applied, and the hydraulic conductivity is set to $1 \times 10^{-6}$ m/s. The figure represents a detailed resolution of a 200 by 200 metre area indicated by the red cross in Figure 4-13.*

the linked-cavity system during the summer months when higher recharge of melt water, both from friction at the bed and from melting at the ice surface, occurs. The calculated through-flow, presented in Figure 4-15, is a result of the assigned boundary conditions but still reflects a realistic pressure field. However, since the pressure is set at 70 % of the overburden ice thickness, the pressure may represent the low end of plausible values.

This pressure field is primarily the result of an upstream lateral boundary condition of 70 % of the ice sheet thickness complemented by the assigned recharge flux. Sensitivity tests showed that the gradient within the local area is such that a 92 % upstream boundary produces the same through-flow for the two upstream specified pressure boundary values in the investigated subarea if the same recharge flux is assigned. The local Darcy velocities within the highly resolved sub-section provide realistic values relative to what has been measured beneath the ice sheet in the GAP project (Chandler et al. 2013, Harper J, personal communication).

Figure 4-16, on the other hand, indicates a cavity system without the well-developed connections. This system would be a more likely winter situation with no surface melt; i.e. during periods with less available melt water. Interestingly, this system distributes water by a strong coupling to the groundwater system beneath. This coupling is, however, in the model controlled by the assigned geological description. In the present model set-up, an approximately 2 metre thick layer at the top is assigned a somewhat higher transmissivity than the deeper bedrock. This description is not unlikely, but rather reflects a commonly observed higher fracture frequency within the first few metres of the rock, especially if horizontally extending fractures are present. These fractures could create the necessary path between the high-pressure "pools" during periods of less water at the interface. Transport between the cavities hence occurs in the subsurface as groundwater flow. The through-flow in the subglacial transmissive layer is reduced by a factor of 2–3, and the pressure field is somewhat higher, see Figure 4-17 (as compared to Figure 4-15).

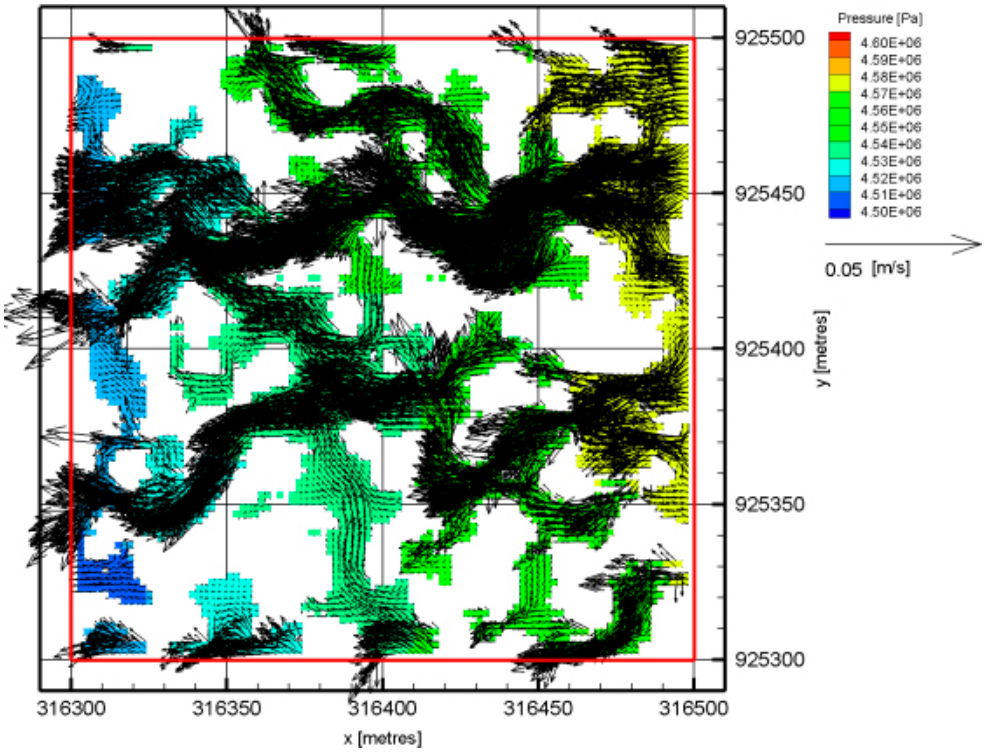


***Figure 4-15.*** *The resulting pressure field in the detailed scale, overlaid by the flow vectors, for a Gaussian multivariate distribution with high connectivity between areas of high flow capacity. Typically, the flow velocities are between $1 \times 10^{-4}$ to $1 \times 10^{-1}$ m/s. A through flux (in the illustration from right to left) of this detailed domain is about 100 l/s. The figure represents a detailed resolution of a 200 by 200 metre area indicated by the red cross in Figure 4-13. The connected system illustrated here can be seen as representative for a "summer" system.*

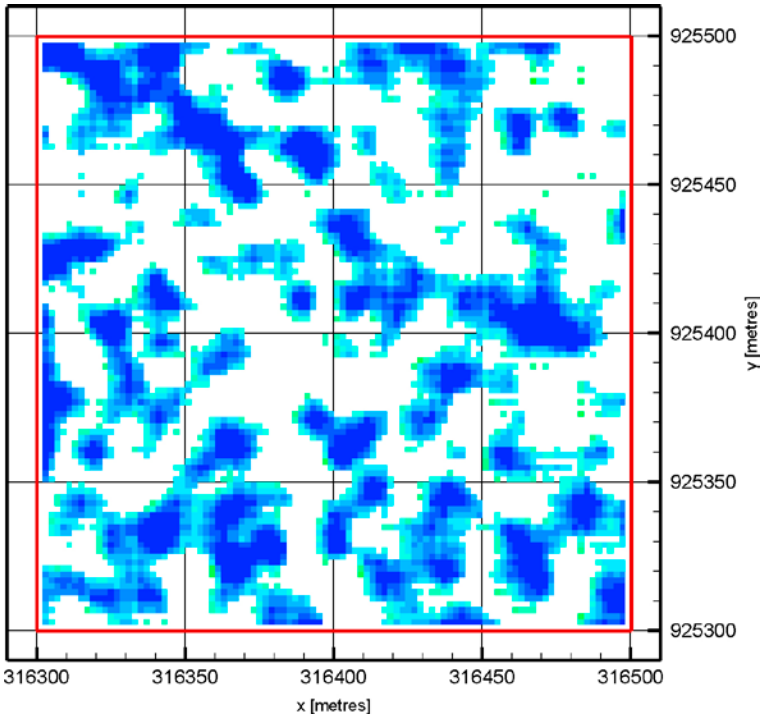


***Figure 4-16.*** *Gaussian multivariate distribution with a correlation length of 8 m. The parts of the generated surface with a hydraulic conductivity smaller than 0.1 m/s were saved and used for detailed groundwater flow analyses. In white areas, a no-flow top boundary condition is applied, and the hydraulic conductivity is set to $1 \times 10^{-6}$ m/s. The figure represents a detailed resolution of a 200 by 200 metre area indicated by the red cross in Figure 4-13.*

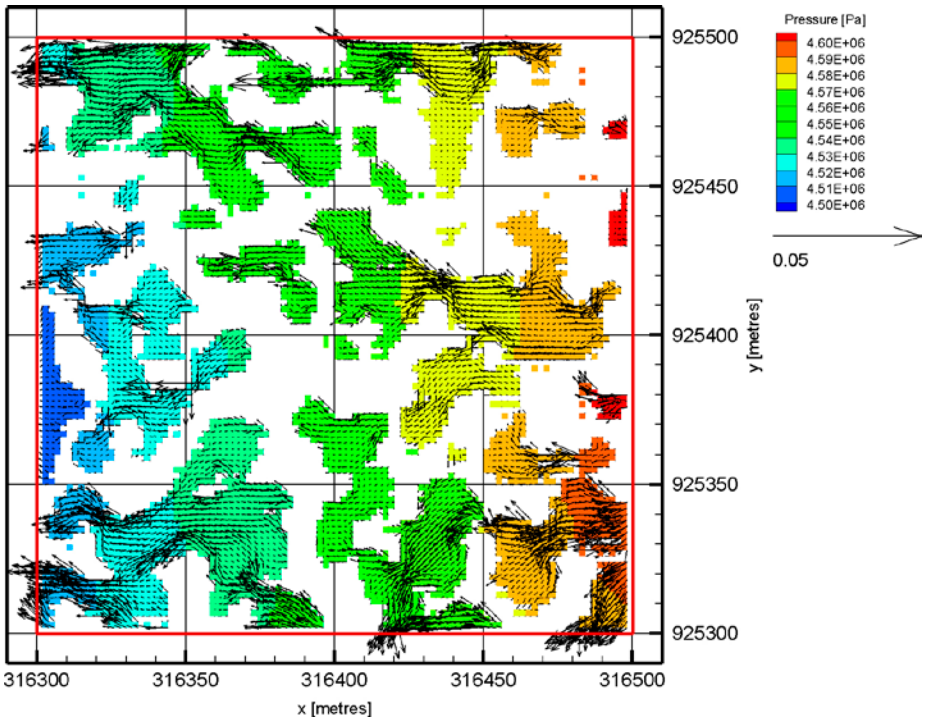


***Figure 4-17.*** *The resulting pressure field in the detailed scale overlaid by flow vectors for a Gaussian multivariate distribution with low connectivity between areas of high flow capacity. Typically, the flow velocities are between $1 \times 10^{-4}$ to $1 \times 10^{-2}$ m/s. A through-flux of this detailed domain is around 35 l/s (in the illustration from right to left). Relative to the other three cases, this surface does not represent a well-connected system. The figure represents a detailed resolution of a 200 by 200 metre area indicated by the red cross in Figure 4-13. This disconnected system can be seen as representative for a "winter" system.*

Alternative distributions, e.g. the tested fractal distribution (Figure 4-19), provides similar results but the pattern does not fit as well with the conceptual ideas of a linked-cavity system. However, this does not by necessity rule out these alternative descriptions since the knowledge of the basal system is limited.

It can be concluded, however, that a uniform flow distribution, as illustrated in Figure 4-21, does not compare well with established understanding of the sub-ice sheet water system at the site. Furthermore, a linked cavity system is not possible during these conditions. A homogeneous flow system could, on the other hand, represent a thin sheet flow.

The sequence from a winter system, described in Figure 4-17, to a constantly evolving summer system similar to what is illustrated in the sequence of Figure 4-15, Figure 4-20, and finally Figure 4-21, is an interesting illustration of the system dynamics as described by Meierbachtol et al. (2013), see Figure 4-18. The figures also illustrate how the development results in a draw downed pressure when the same boundary conditions are applied, i.e. same amount of water during summer as well as in winter. Note that Figure 4-20 indicates "straight" channel-like features and that this system could evolve into a tunnel system instead of into the now-illustrated change to thin sheet flow. This latter development is more likely but harder to model within the same conceptual framework, and is hence only mentioned in the present context.

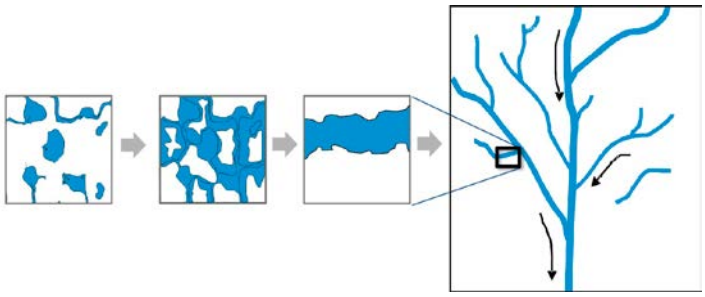

***Figure 4-18.*** *Illustration of the development from a disconnected system into a channelized network.*

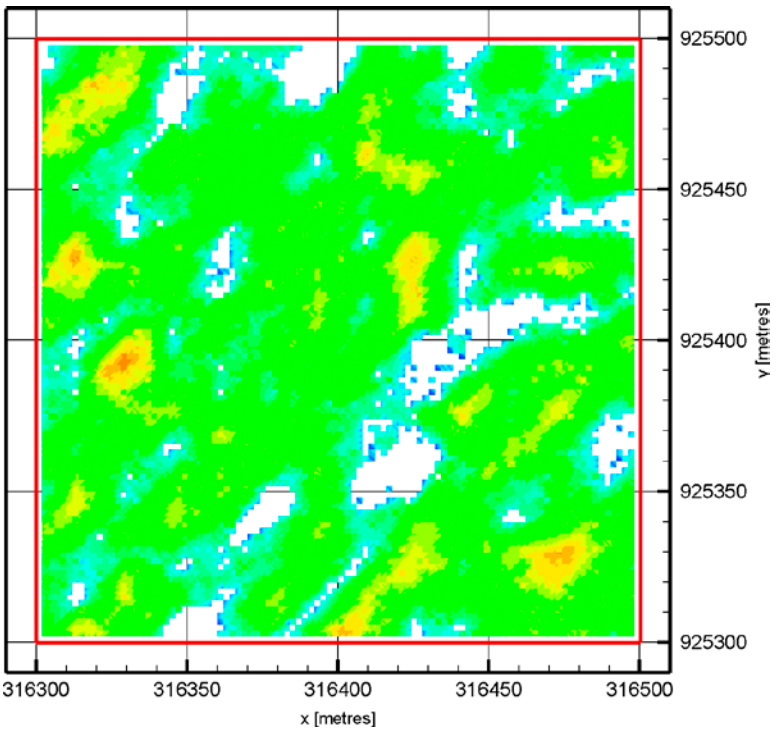


***Figure 4-19.*** *Fractal distribution with an initial length scale of 16 m. The length scale can be compared to a correlation length. The parts of the generated surface with hydraulic conductivity larger than 0.1 were saved and used for detailed groundwater flow analyses. In white areas, a no-flow top boundary condition is applied, and the hydraulic conductivity is set to* $1 \times 10^{-6}$ *m/s. The figure represents a detailed resolution of a 200 by 200 metre area indicated by the red cross in Figure 4-13.*

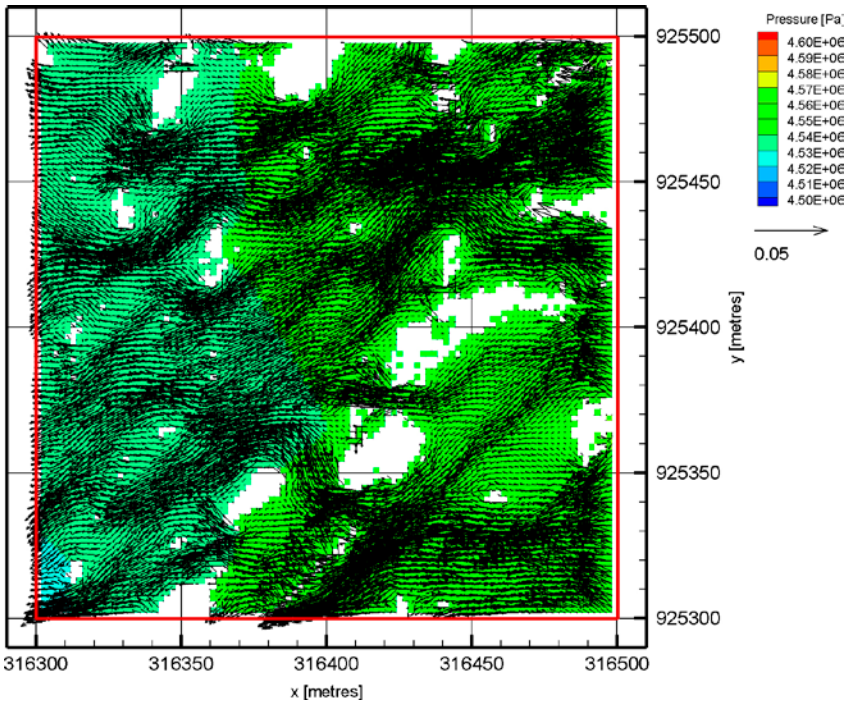


***Figure 4-20.*** *The resulting pressure field in the detailed scale overlaid by flow vectors, for a Fractal distribution with very high connectivity between areas of high flow capacity. Typically, the flow velocities are between $1 \times 10^{-2}$ t0 $1 \times 10^{-1}$ m/s. A through-flux of this detailed domain is around 200 l/s. The figure represents a detailed resolution of a 200 by 200 metre area indicated by the red cross in Figure 4-13. The system is basically completely uncoupled from the ice sheet and could be viewed as either a sliding ice sheet or as a large portion of the bed being almost as a thin continuous film of water.*

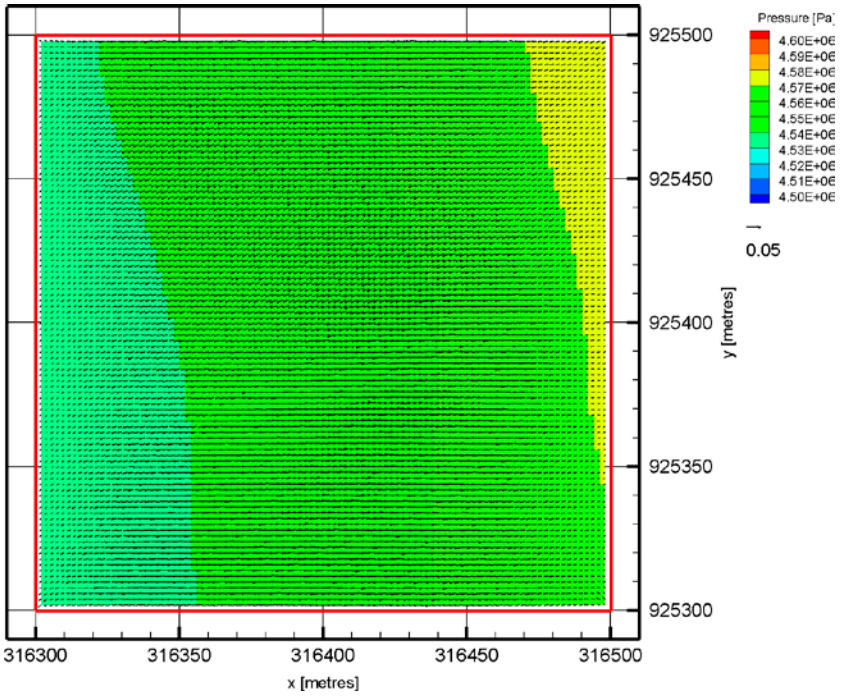


***Figure 4-21.*** *The resulting pressure field in a perfect homogeneous description of the transmissive layer in and outside of the detailed scale overlaid by flow vector, for a homogeneous distribution with a uniform and high flow capacity. Typically, the flow velocities are between $1 \times 10^{-2}$ to $1 \times 10^{-1}$ m/s. A through-flux of this detailed domain is about 280 l/s. The figure represents a detailed resolution of a 200 by 200 metre area indicated by the red cross in Figure 4-13. The regional flow field in Figure 4-13 explains the somewhat uneven flow and pressure distributions shown even if the tranmissive layer in the detailed scale model is perfectly homogeneous.*

## 4.6 Part II data

In addition to data used in Part I, the input data for Part II were based on:

- DEM data: ASTER GDEM version 1 (https://asterweb.jpl.nasa.gov/gdem.asp) and Geo Radar data from the GAP (Lindbäck et al. 2014).
- Ice thickness data: GIMP DEM version 1 (Howat et al. 2014).
- Deformation zone model (Engström et al. 2012, Follin et al. 2011).
- Fracture data: Stochastic data generated based on Laxemar data (Follin et al. 2011)[4].

Along with relevant site specific data presented in Harper et al. (2011), such as pressure observations, some borehole transmissivity values, etc.

## 4.7 Part II data processing

Figure 4-22 shows the data available for discretization of the DEM during the Part II studies for the studied model domain. Figure 4-23 illustrates the resulting surface after a refining of the DEM from the available data down to a uniform 20 m scale. The data processing was conducted in the software Surfer using the predefined set-up of the Surfer kriging routine. The routine creates a smooth surface while honouring values at positions where data exist in the original DEM.

Comparing Figure 4-23 and Figure 4-24 illustrates the importance of input data. The latter figure presents the surface used in Part I, based on the Bamber 1993–1999 data set, and it is clear not only how big the differences are but also how an overly sparse data set misses essential topographical differences like local thresholds and recharge/discharge characteristics.

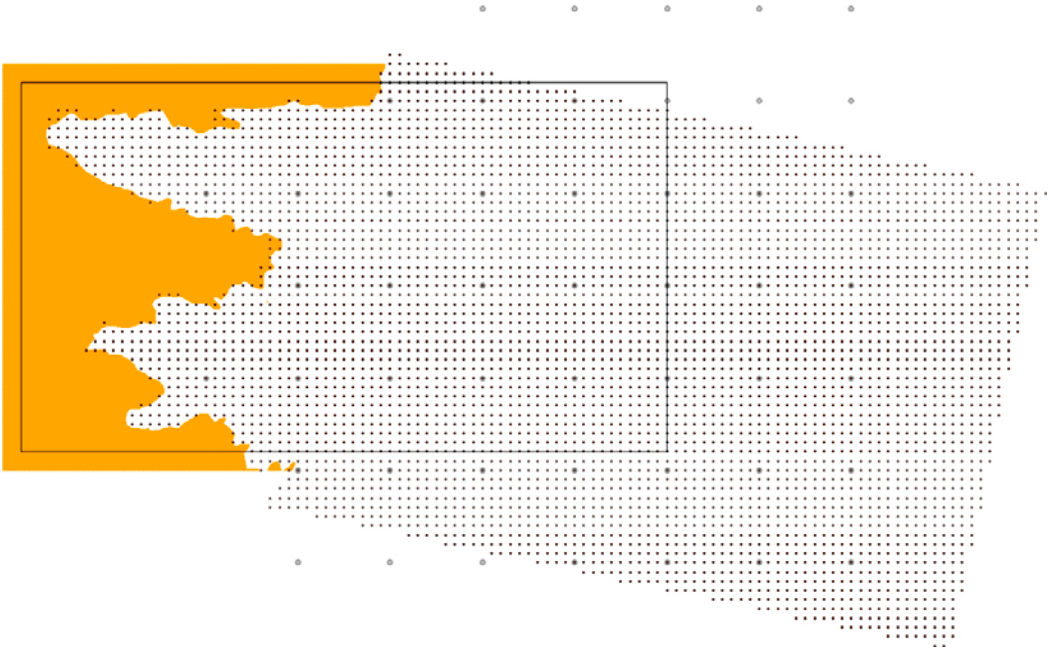

***Figure 4-22.*** *Data points available for the DEM in the Part II studies. Orange dots = ASTER GDEM, Small dots = GIMP DEM, large dots = Bamber 1993–1999 data. Note that the ASTER GDEM data points (orange) are so dense that they look like a continuous surface.*

[4] At the initiation of work described in part II of the present report, the geological setting of the GAP site was known to be more similar to the Laxemar site. In order to be more site specific, it was consequently decided to change the input data set from the Forsmark site to the Laxemar site.

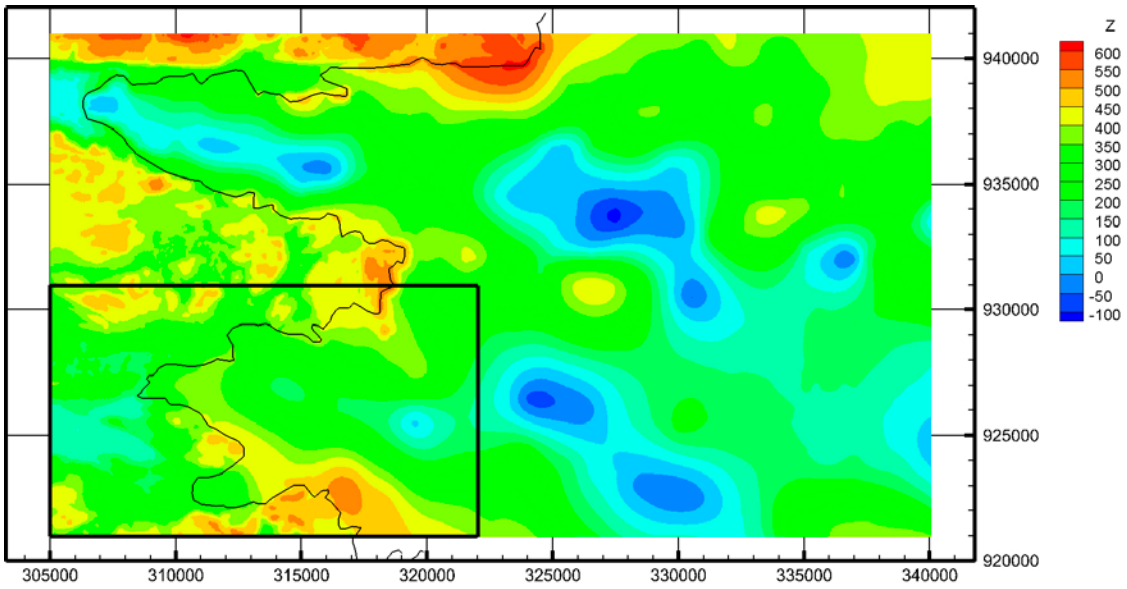


***Figure 4-23.*** *Illustration of the resulting DEM surface used in the Part II studies. Thin black line indicates the assumed position of the ice margin.*

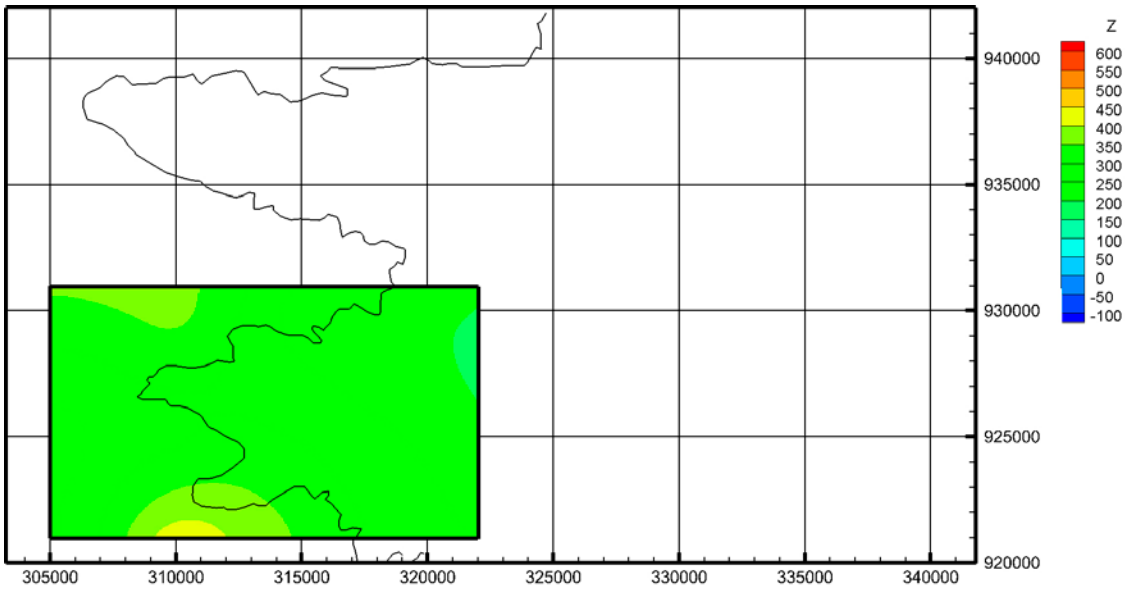


***Figure 4-24.*** *Illustration of the resulting DEM surface used in the Part I study. Illustration intended for comparison with Figure 4-23. Thin black line indicates the assumed position of the ice margin*

Figure 4-25 shows as coloured lines the deformation zone model by Engström et al. (2012) used in this study. The deformation zone model is deterministic and incorporates site-specific data. However, the orange-brown coloured lineaments, in the ice sheet part of the domain, are not true lineaments, but a reproduction of the lineaments in the ice marginal area. The strategy of the adopted approach is explained in Follin et al. (2011).

Figure 4-26 shows two cross-sections of the model. The left panel illustrates the deformation zone model within the studied model domain. The right panel illustrates the generated stochastic fracture network overlaying the deformation zones in the model domain. All fractures shown, deterministic as well as stochastic, are connected. Isolated features are removed from the simulation.

Figure 4-27 illustrates the modelled fractures that cross the centre line of the DH-GAP04 borehole. The frequency of generated fractures is quantitatively compared to measured data (Harper et al. 2016) with acceptable results. This indicates that the adopted Laxemar fracture statistics are relevant.

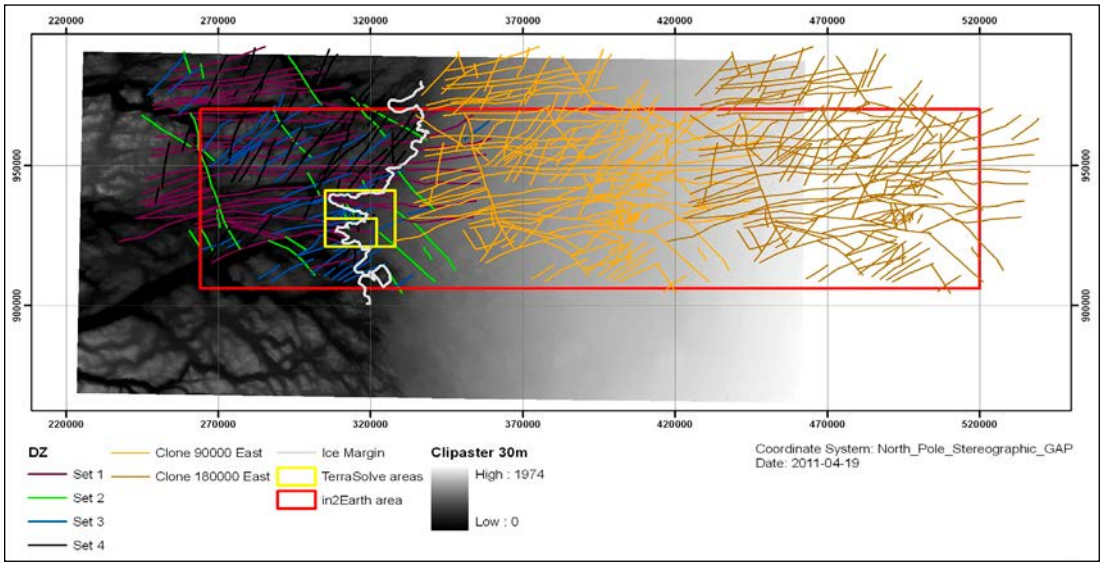


***Figure 4-25.*** *Illustration of the deformation zone model (Engström et al. 2012). The model domains used by In2Earth (Jaquet et al. 2012) are shown for comparison. White line indicates the position of the ice margin.*

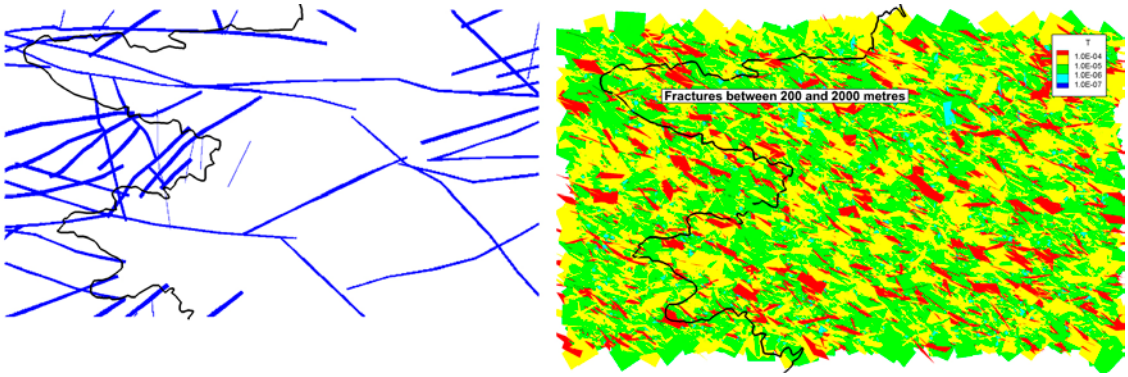


***Figure 4-26.*** *Left) Illustration of the deformation zone model (Follin et al. 2011) that applies to the model domain of Part II. Right) Illustration of the stochastic fractures contained within the same model domain. The black line indicates the ice sheet margin.*

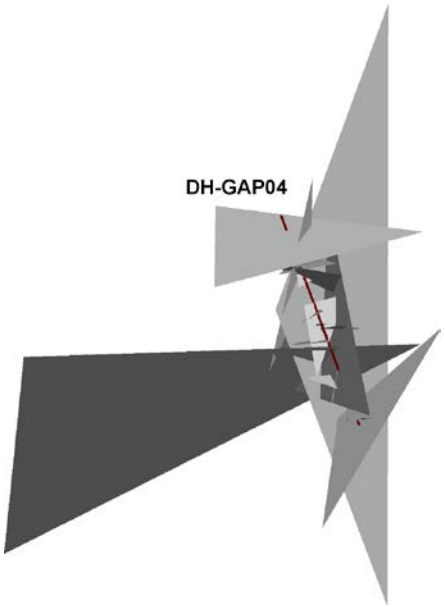


***Figure 4-27.*** *Illustration of all simulated fractures that cross the centre line of the DH-GAP04 borehole.*

## 4.8 Part II boundary conditions

In Part II the "realism" aimed for in Part I was abandoned in favour of a traditional hydrogeological top boundary condition specifying the pressure (Dirichlet boundary condition). The study within Part II focuses on uncertainties in fluxes and primarily on potential glacial melt water discharge to the Talik lake (see Figure 1-2 and e.g. Figure 4-28).

Combinations of different sub-glacial permafrost extents and sub-glacial top boundary pressures were used. The following set-ups were tested:

- 92, 70, 50, 30 % of overburden ice thickness was assigned as specified pressure.
- Sub-glacial permafrost is assigned if the ice sheet thickness is less than 0, 100, or 200 metres. The correlation of assigned negative temperatures and ice thickness is only a modelling choice but contains a certain amount of realism since thicker ice sheets provide a better insulation for the bed from cold air.

The conditions chosen here are an open issue especially concerning the sub-glacial permafrost, and that this study will address the particular case of relict frozen ground below the ice/bed interface. The data from GAP (Harper et al. 2016) suggests, however, that the ground interface beneath the ice sheet is at melting temperatures.

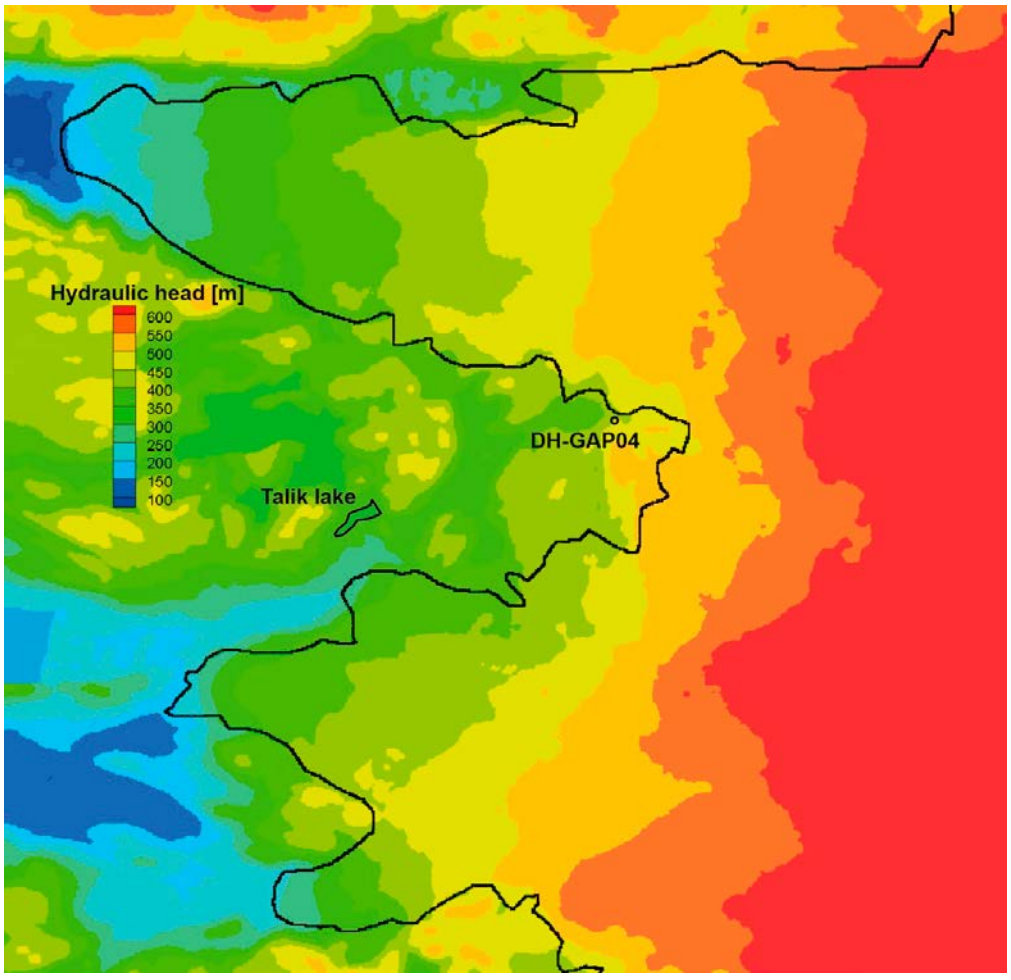


***Figure 4-28.*** *Illustration of the top boundary pressure situation for a case were sub-glacial pressures are 92 % of ice thickness and the periglacial forefield is assigned a groundwater table at the surface. Permafrost, or more correctly ground surface temperatures below zero degrees, is assigned in the periglacial forefield with exception of taliks. Sub-glacial temperatures are just above zero (0.1 Degrees Centigrade). Black line indicates position of the ice margin.*

Figure 4-28 and Figure 4-29 illustrate two of the above combinations. The first combination assumes frozen ground conditions in front of the ice sheet except in taliks. This assumption results in a permafrost layer in three dimensions. At depth beneath a warm based surface, i.e. in a talik or below a warm-based ice sheet, the permafrost reaches in beneath the warm body. If a talik is small enough, it could potentially be closed under such circumstances. This, however, never happens to the lakes assigned as taliks in the present study due to the fact that beneath the ice sheet, the temperature is assigned to just above zero degrees Centigrade (0.1 °C) i.e. almost at pressure melting[5], while beneath the taliks, the temperature is set to 4 degrees centigrade. Figure 4-29 illustrates the conceptual idea that frozen ground reaches in under the ice sheet and affects sub-glacial ground; in the present case, effect is seen until the overburden ice thickness reaches a thickness of 200 metres. All frozen ground and talik locations are assigned a specified pressure equal to the ground or lake surface (according to the DEM).

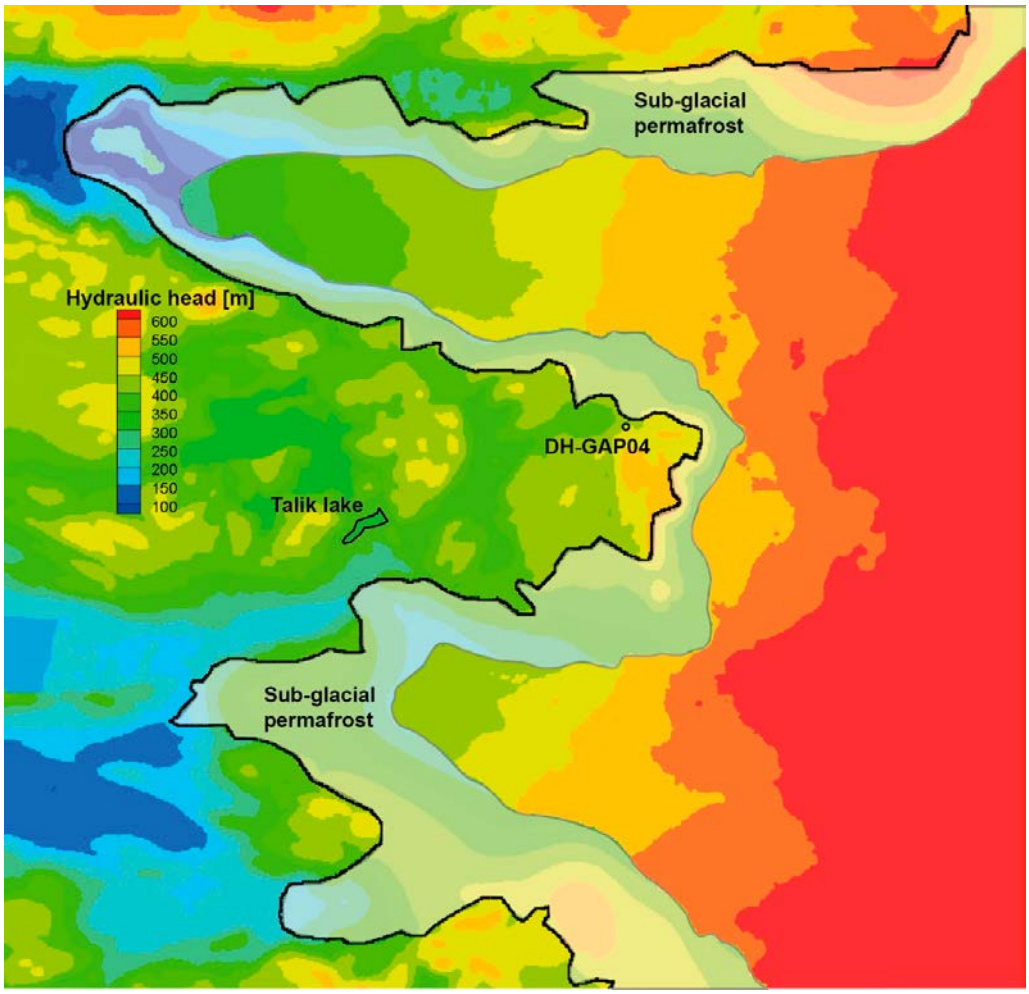


***Figure 4-29.*** *Illustration of the top boundary pressure situation for a case were sub-glacial pressures are 92 % of ice thickness. The periglacial forefield as well as sub-glacial ground with negative temperatures are assigned a groundwater table at the surface. Permafrost, or more correctly ground surface temperatures below zero, is assigned in the periglacial forefield with exception of taliks and sub-glacially where the ice sheet thickness is less than 200 metres. Sub-glacial temperatures elsewhere are just above zero (0.1 Degrees Centigrade). Black line indicates position of the ice margin.*

[5] In the adopted model, no dependence of pressure on the freezing point is modelled in order to minimise the non-linearity of the problem. In the relatively thin ice sheet of the region, the modelling focuses on, this assumption should result in a negligible difference between the actual temperature (sub-zero) and the one assigned in the model (0) for pressure melting.

## 4.9 Part II results

An extra outcome of the Part II work is that the upscaled transmissive surficial layer and the uppermost part of the groundwater system can be illustrated. It can be concluded that the upscaling destroys the realistic patterns (see Figure 4-30) of a transmissive layer on a metre scale. This indicates that if one's main interest lies on transport pathways and local routing in the transmissive layer and uppermost groundwater system, then a high resolution model is indeed needed. However, the upscaled and locally highly resolved model seems to produce similar pressure distributions already at relatively shallow depths. Hence, the effect on the deep groundwater flow seems to be reproduced irrespective of the model resolution chosen for the surficial parts. The obtained result is useful since it strongly indicates that a specified pressure top boundary condition is sufficient if the main interest is in deep (repository depth, i.e. around 500 metres) groundwater circulation.

As described in Section 1.2, the scope and objectives of Part II are somewhat different from Part I. Part II primarily focuses on providing some initial results on detailed regional flow behaviour of the Talik lake (referenced as Talik 113 in Figure 4-31). The main interest is to confirm if the Talik Lake could act as a discharge zone for glacially induced melt water.

The simulations were conducted as sensitivity studies using different applied specified pressures beneath the ice sheet, as well as different amounts of sub-glacial permafrost, extending from the ice margin and inwards, in all cases.

In all cases of varying sub-glacial pressure (30, 70 or 92 % of ice overburden pressure), a weak flow signal from beneath the ice sheet towards the Talik lake is apparent (see Figure 4-32). However, with successively lower pressures beneath the ice sheet this effect becomes smaller, and if the specified pressure is only some 30 % of the ice thickness, the pattern and direction of the pathlines may equally well indicate a groundwater flow controlled by local pressure gradients. This would imply groundwater flow through the frozen ground, which is a consequence of the non-zero, but low, permeability of frozen ground. However, as shown in Figure 4-33, sub-glacial permafrost extending significantly from the ice margin and in beneath the ice sheet, more or less completely turns off the regional flow towards the Talik lake (this is seen by the almost non-existing black lines in Figure 4-33). This clearly indicates that the ice sheet provides flow to the Talik lake and discharge of glacially induced melt water should be expected. However, it also indicates that the amount is strongly dependent on sub-glacial permafrost and the sub-glacial pressure. Both of these are likely to change significantly during any specific year as well as over longer time scales. Note that the pathlines are simulated for a period of 10 000 years (of steady-state conditions) and that none of the pathlines, irrespectively of the applied specified pressure, reach all the way from the Talik lake to any sub-glacial location during the conducted particle back-tracking.

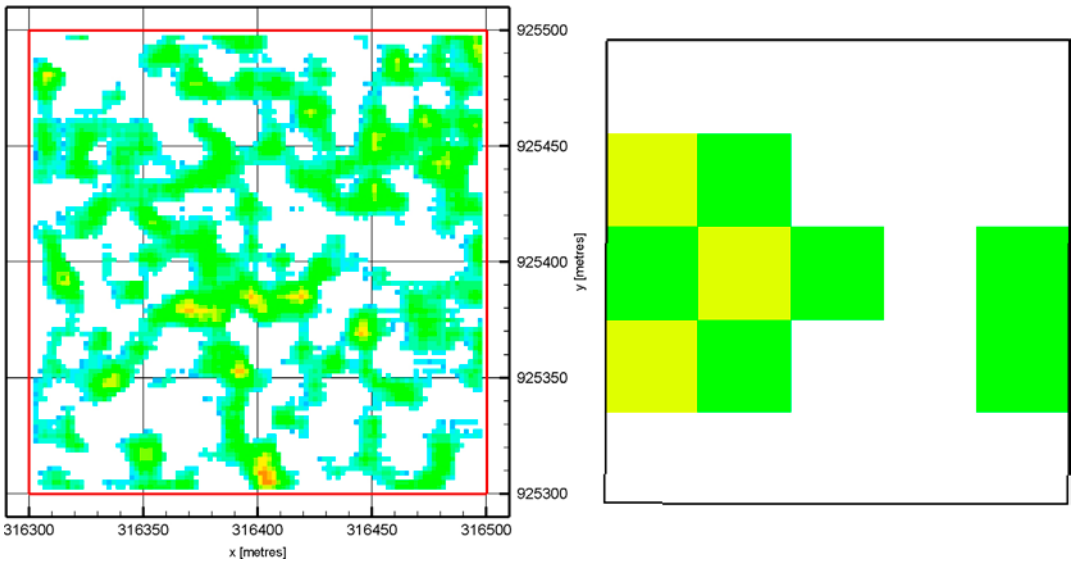


***Figure 4-30.*** *Comparison of the local hydraulic conductivity viewed using the same colour scale for the (left) high resolved sub-section (same as Figure 4-14) and (right) upscaled conductivity of the same sub-volume.*

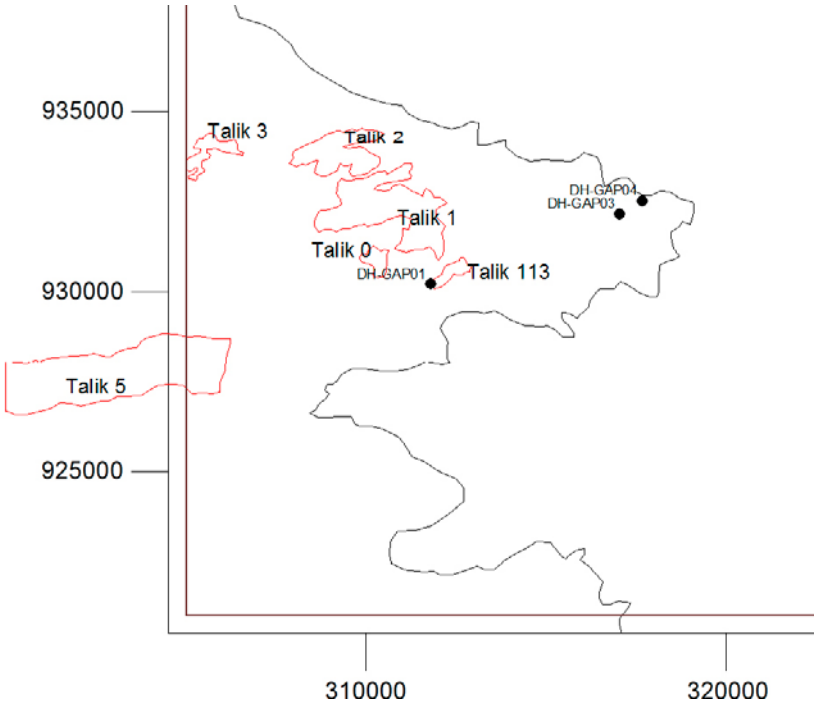


***Figure 4-31.*** *Illustration of the different taliks modelled and their location in relation to the ice sheet margin (delineated by a black line) and the three GAP boreholes. The numbering associated with the taliks, i.e. Talik 0, Talik 1, …, Talik, 113 is simply the digitalised order of the taliks.*

Particles are released uniformly over the entire lake surface and are backtracked. No forward tracking is conducted in the present work. A few results are of special interest:

First, it is noted that only particles released on the northeast part of the lake yield pathlines during the backtracking. On the southwestern part of the lake, the released particles stand still, indicating that this part of the Talik lake provides recharge to the groundwater system, most likely draining towards the much lower elevated lake, Talik 5 in Figure 4-31. However, only backtracking has been conducted and further analyses including forward tracking are needed in order to verify this result.

Second, the particles released in the part of the Talik lake located closest to the nearby lake, Talik 1 in Figure 4-31, all indicate a gradient from the nearby lake which is approximately 10 metres higher, possibly indicating a slow transport between different taliks. Such transport would be stronger if the differences in lake elevations were larger.

It should be noted that all these results are related to deep groundwater flow beneath or possibly within frozen ground. No active layer flows are modelled here.

A second focus of the Part II work is to investigate in detail the DH-GAP04 borehole. This is also done for the different sensitivity cases described above.

Figure 4-34 presents the resulting fresh water head along the borehole for a case with no sub-glacial permafrost (note that the permafrost extends to some distance, approximately 100 metres, as a wedge beneath the ice sheet at depth). The hydraulic head along the borehole ranges from approximately 473 metres at depth, and 472 metres at the base of the permafrost. Just beneath the permafrost, a hydraulic head of 473 metres is obtained in the model; this head decreases about 1 metre for the middle part and then increases again to 473 metres. Hence, there is spatial variation in the borehole due to changes in geology, but the variation is much smaller than the encountered temporal variation in DH-GAP04 of about 30 metres (Claesson Liljedahl et al. 2016). In the present model set-up, the bedrock is too permeable and connected in order to provide more distinct differences between different parts of the borehole. The resulting hydraulic head of 470 metres is in reasonably good agreement with the encountered hydraulic head in the lower parts of the borehole, and likely reflects a regional flow gradient from the ice sheet interior towards the Talik lake; a simplified illustration is provided in Figure 4-35.

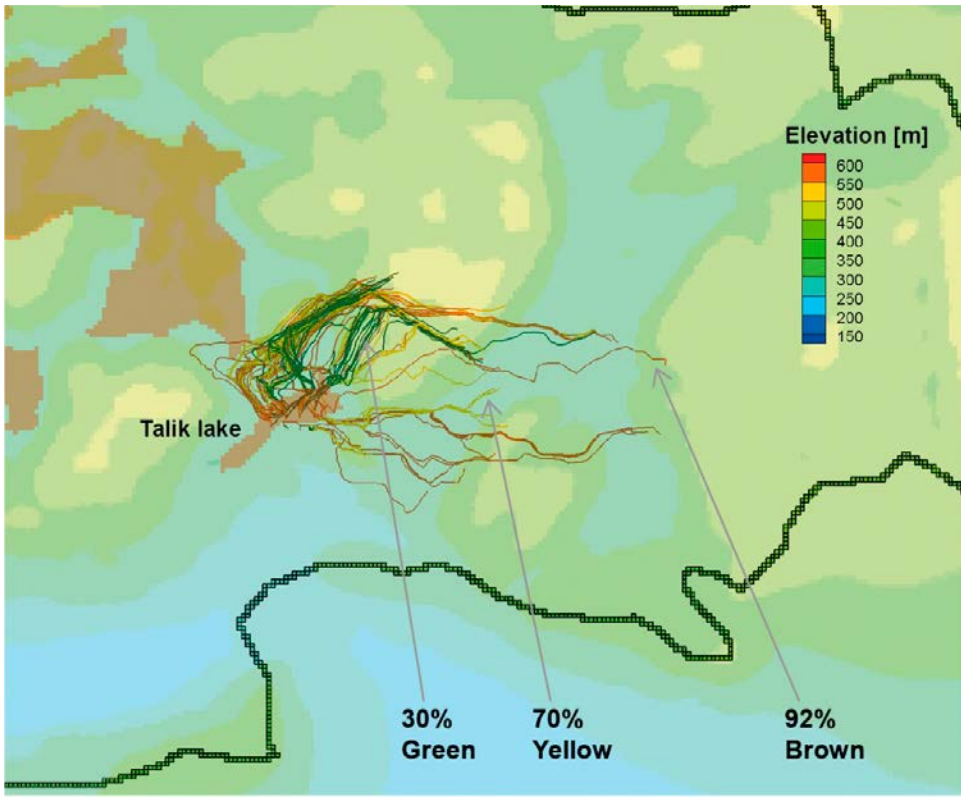


***Figure 4-32.*** *The resulting pathlines for three cases which all have no sub-glacial permafrost and different specified sub-glacial pressures (30 %, 70 %, and 92 % of ice thickness). The line of green cells indicates the ice sheet margin. Brownish shade indicates talik lakes.*

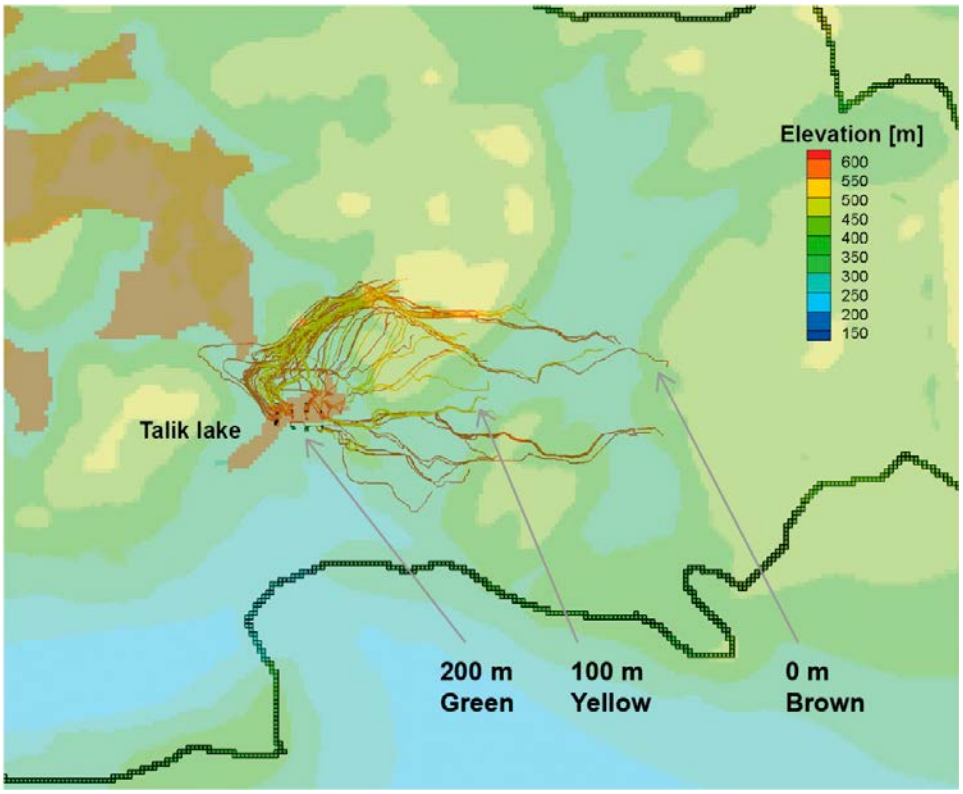


***Figure 4-33.*** *The resulting pathlines for three cases which all have 92 % of ice thickness as specified pressure, and different sub-glacial permafrost defined by 0, 100, or 200 metres of ice thickness. Brownish shade indicates talik lakes.*

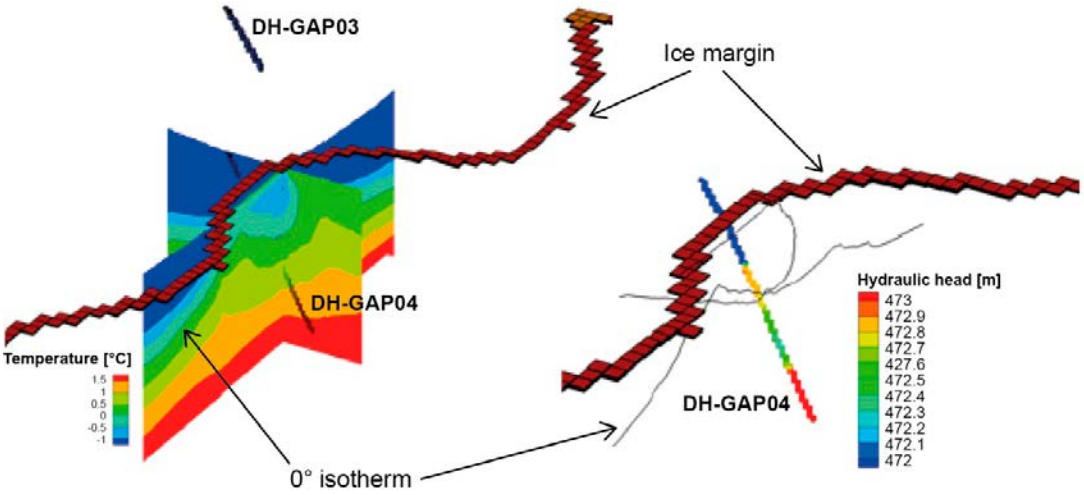


***Figure 4-34.*** *The resulting temperature (left) and fresh water head [m] (right) in the DH-GAP04 borehole for a simulated case of no sub-glacial permafrost and 92 % of ice thickness as specified pressure. The line of reddish cells indicates the ice sheet margin.*

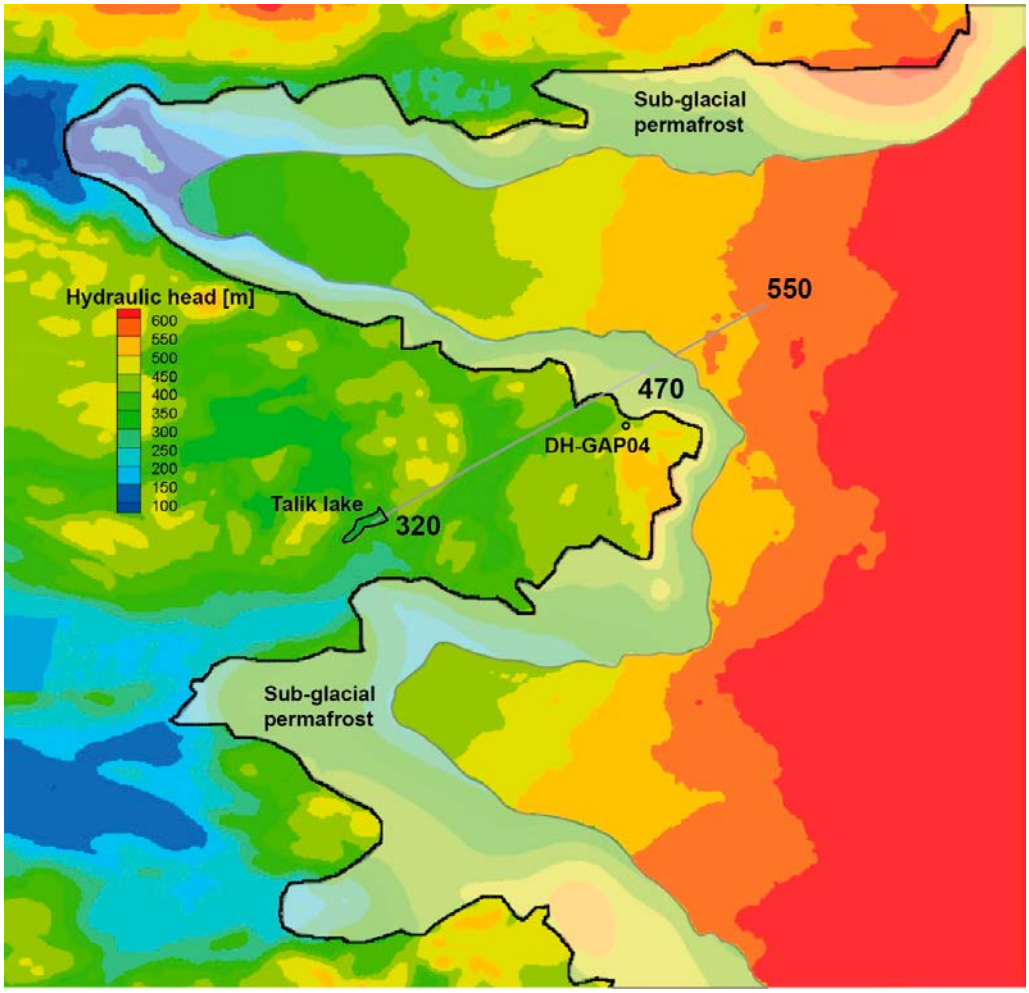


***Figure 4-35.*** *Simplified illustration of a possible regional flow gradient (550 metres of hydraulic head at ice sheet interior and 320 metres of hydraulic head is the Talik lake elevation) and resulting head at the DH-GAP04 borehole area. The head of 470 metres is in reasonable agreement compared to the encountered head in the deep section of the borehole (Claesson Liljedahl et al. 2016). Black line indicates position of the ice margin.*

Figure 4-36 presents similar results but for a case where the permafrost extends further in beneath the ice sheet. Interestingly, the resulting pressure along the borehole is approximately 60 metres lower for this case. This result is most likely an effect of the applied specified pressure boundary beneath the ice sheet. Specifically, the pressure is specified at ground surface in the frozen part, and even if the permafrost has a lowered permeability, a through flow is still possible. Thus, this case creates an extreme gradient at the permafrost fringe beneath the ice sheet as seen in the sharp contrast in pressure along the permafrost interface as illustrated in e.g. Figure 4-35.

These model results indicate that the permafrost does not extend far in beneath the ice sheet and also that the model needs to be further developed in terms of discrete fracture behaviour in order to more correctly reproduce the encountered behaviour in DH-GAP04.

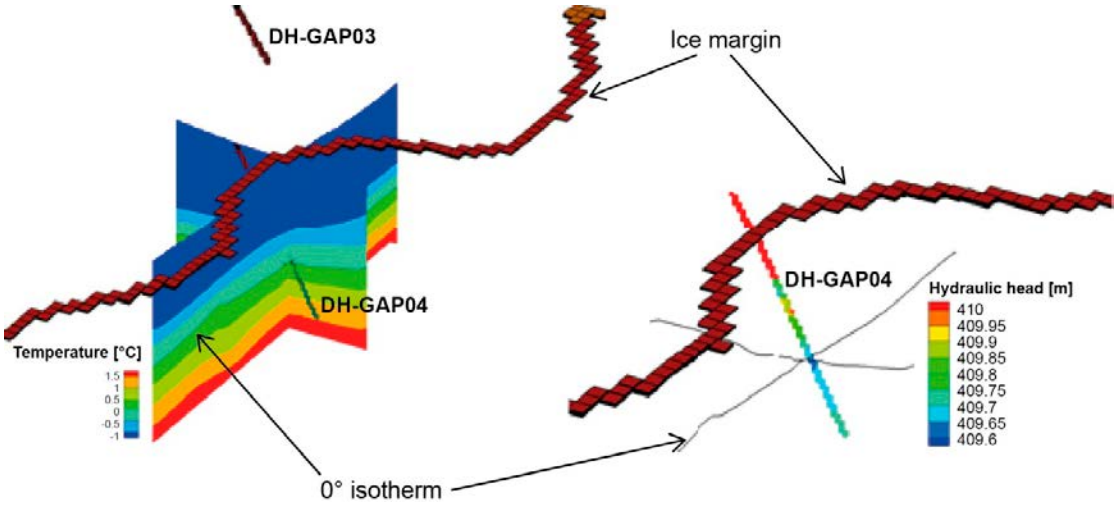


***Figure 4-36.*** *The resulting temperature (left) and fresh water head [m] (right) in the DH-GAP04 borehole for a simulated case of permafrost extending further in under the ice sheet (the 200 metre ice thickness case) and 92 % of ice thickness as specified pressure. The line of reddish cells indicates the ice sheet margin.*

# 5 Conclusions and recommendations

The objective of the GAP geosphere modelling is to *investigate the conditions and processes that impact the recharge of glacial melt water into the geosphere, in particular to repository depth in a fractured crystalline rock and over safety assessment time scales.* Specifically, it is the recharge of dilute and oxygenated glacial melt waters to repository depth that is of most relevance as this represents a significant change to the sub-surface conditions needed to safeguard the integrity of the engineered barriers.

The work was divided into two parts.

Part I tried to:

- investigate the influence of recharge variations on the groundwater flow and pressures in a sub-glacial environment, and
- investigate the relevance of large-scale groundwater flow models' top boundary conditions, i.e. in general, a specified pressure condition.

In order to address these questions, a conceptual idea of the transmissive layer at the interface between the ice sheet and the geological bed beneath was developed. The transmissive layer was conceptualized using a statistical distribution centred on a high value (1 m/s) of hydraulic conductivity. It may be concluded that the applied Gaussian distributions, which connects high conductivity paths, provides a good means of generating realistic sub-glacial melt rates for use as a top boundary condition. Also, the transmissive layer yields realistic and measureable sub-glacial pressures mostly close to the floatation pressure, i.e. 92 % of the ice thickness (overburden).

The presented results indicate that the pressure differences between a well-connected transmissive layer (which could be interpreted as a summer drainage system) and a poorly connected transmissive layer (a winter drainage system) are not so large. The poorly connected system has slightly higher pressures, but significantly lower Darcy velocities. However, even the poorly connected system is connected if the geological substratum is at least somewhat permeable; hence the flow between "pools" in the transmissive layer are routed through the geological medium as groundwater. However, the generality of this conclusion is still to be substantiated since the simulated system has only a small internal volume at the very high resolution and all the surrounding boundary conditions are maintained during all simulated variants of the detailed scale.

However, bearing the last statement above in mind; the findings of the present study further indicate that the pressure at depth is rather insensitive to the character and behaviour of the transmissive layer. It is however postulated that in a dynamic system where the transmissive layer is evolving and rapidly changing along with the available water at the sub-glacial interface, also pressure at depth will vary. Results from the GAP (Claesson Liljedahl et al. 2016) illustrate such pressure changes in a borehole at great depth. However, this borehole is found at the ice sheet margin; the marginal area is the area most likely to have significant changes over the year. The present results illustrate that the marginal area is always close to the floatation pressure and only a minor change in available recharging waters will create over-pressures and unstable ice sheet conditions.

The Part II work had a slightly different approach, leaving the process-based top boundary conditions and instead performing some sensitivity studies on the traditional type of top boundary conditions, i.e. specified pressure, and sub-glacial permafrost. In this context the simulations aimed at:

- providing a first set of supporting regional scale modelling of recharge and discharge in taliks found in the periglacial forefield, and
- investigating the flow and pressure system within the assessed model around the DH-GAP04 cored borehole.

The results of the present study indicate that glacially induced melt water recharge beneath the ice sheet, and discharge in taliks in front of the ice sheet margin, is apparent in the periglacial environment. The sensitivity study indicates that both the specified sub-glacial pressures, and the amount

of sub-glacial permafrost, affect the rate of discharge. However, it appears that the discharge rate is most sensitive to the distribution of sub-glacial permafrost. It should be noted that these results are dependent on the particular model specifications and hence may be model specific. However, irrespective of this potential model dependence, the results have been helpful in that they provide insight into the discharge characteristics of sub-glacially recharged melt waters. Discharge in taliks is not only possible but most likely realistic also relatively far away, and also at topographical elevations exceeding the ice sheet margins elevation.

Furthermore, the results indicate that taliks may act as both recharge and discharge locations. Even if a talik may be interpreted as a point pressure in nature and hence should act either as a recharge or discharge location, it should, however, be noted that a taliks may have quite large areal extents and also connect to the regional groundwater flow system at depth. This regional flow system is likely to have a gradient that may be little affected by the talik above. Hence, the talik lake elevation could respond to different pressure situations beneath its surface due to the regional pressure distribution at depth. Thus, in a regional context it seems plausible that a talik would be able to contain both recharge and discharge locations within it.

The detailed results of the DH-GAP04 borehole indicate sensitivities to the amount of sub-glacial permafrost. The results do not indicate any large pressure variations along the borehole, as observed in the field measurements, but this is likely an artefact of the porous media approach adopted. Further studies are needed to provide further insight into this matter; however, it may be concluded that the deepest parts of the borehole respond to the large-scale regional flow and pressure fields.

A final conclusion, based on the performed work, is that topography provides a strong control on glaciated groundwater systems. In line with what was shown in Vidstrand et al. (2013) concerning geological details, the current results indicate that in order to obtain an understanding of details also at great depth, a good representation of the topography is needed. Hence, models of super-regional extent and low resolution should be carefully assessed while investigating details. Furthermore, even if a specified pressure boundary condition may seem to be a relevant boundary condition for these types of problems, it should be used with care when the topographic relief is significant. For particular settings, resolution that is too coarse may result in “pot holes” in the sub-glacial environment, which then will act as “unknown and unrealistic sinks” in the flow model. A specified pressure boundary condition appears more appropriate in topographically flatter regions such as the potential sites for deep geological storage of nuclear waste in Sweden and Finland.

Based on the presented work and conclusions drawn, the following conclusions can be drawn and hence provide recommendations for future work are suggested:

- For simulations of deep groundwater systems, a specified pressure top boundary condition is valid and useful. However, in order to successfully adopt this simplified top boundary condition, knowledge of local topography as well as the extent of sub-glacial permafrost is important.
- For details on sub-glacial groundwater flow and melt water flow within a transmissive layer, it is important to resolve the model of interest. Upscaling of this layer is complicated if even possible.
- The presented results indicate that taliks in a periglacial environment may receive flow governed by subglacial discharge, i.e. taliks act as discharge zones. However, taliks may also provide recharge to the deeper groundwater system; this will depend on the relative locations within a talik, and on its relation to other taliks and the ice sheet.

Two main areas for further modelling work within the GAP are identified:

- More details on recharge and discharge patterns in taliks should be explored with a more focused model.
- More focused models incorporating site-specific geology and other site-specific information (i.e. The Pingo, lake tapping etc.) are needed for further detailed modelling of local details such as e.g. DH-GAP04 site.

# References

SKB's (Svensk Kärnbränslehantering AB) publications can be found at www.skb.com/publications.


**Anderson D M, Tice A R, 1973.** The unfrozen interfacial phase in frozen soil systems. In Hadas A, Swartzendruber D, Rijtema P E, Fuchs M, Yaron (eds). Physical Aspects of Soil Water and Salts in Ecosystems. Berlin: Springer-Verlag. (Ecological studies 4), 107–124.

**Anderson M P, Woessner W W, 1992.** Applied groundwater modeling: simulation of flow and advective transport. San Diego, CA: Academic Press.

**Anderson N J, Bennike O, Christoffersen K, Jeppesen E, Markager S, Miller G, Renberg L, 1999.** Limnological and palaeolimnological studies of lakes in south-western Greenland. Geology of Greenland Survey Bulletin 183, 68–74.

**Bennike O, 2000.** Palaeoecological studies of Holocene lake sediments from west Greenland. Palaeogeography, Palaeoclimatology, Palaeoecology 155, 285–304.

**Bense V F, Person M A, 2008.** Transient hydrodynamics within intercratonic sedimentary basins during glacial cycles. Journal of Geophysical Research 113, F04005. doi:10.1029/2007JF000969

**Bosson E, Sabel U, Gustafsson L-G, Sassner M, Destouni G, 2012.** Influences of shifts in climate, landscape, and permafrost on terrestrial hydrology. Journal of Geophysical Research 117. doi: 10.1029/2011JD016429

**Bosson E, Selroos J-O, Stigsson M, Gustafsson L-G, Destouni G, 2013.** Exchange and pathways of deep and shallow groundwater in different climate and permafrost conditions using the Forsmark site, Sweden, as an example catchment. Hydrogeology Journal 21, 225–237.

**Boulton G S, de Marsily G, 1997.** Hydrogeological aspects of glaciation. In King-Clayton L, Chapman N, Ericsson L O, Kautsky F (eds). Glaciation and hydrogeology. Proceedings of the workshop on the impact of climate change and glaciations on rock stresses, groundwater flow and hydrochemistry – past, present and future. Hässelby, Sweden, 17–19 April 1996. SKI Report 97:13, Statens kärnkraftinspektion (Swedish Nuclear Power Inspectorate).

**Boulton G S, Payne A, 1993.** Simulation of the European ice sheet through the last glacial cycle and prediction of future glaciation. SKB TR 93-14, Svensk Kärnbränslehantering AB.

**Boulton G S, Slot T, Blessing K, Glasbergen P, Leijnse T, van Gijssel K, 1993.** Deep circulation of groundwater in overpressured subglacial aquifers and it's geological consequences. Quaternary Science Reviews 12, 739–745.

**Boulton G S, Caban P E, van Gijssel K, 1995.** Groundwater flow beneath ice sheets: Part I – Large scale patterns. Quaternary Science Reviews 14, 545–562.

**Boulton G S, Caban P E, van Gijssel K, Leijnse A, Punkari M, van Weert F H A, 1996.** The impact of glaciations on the groundwater regime of Northwest Europe. Global and Planetary Change 12, 397–413.

**Boulton G S, Caban P, Hulton N, 1999.** Simulations of the Scandinavian ice sheet and its subsurface conditions. SKB R-99-73, Svensk Kärnbränslehantering AB.

**Boulton G S, Lunn R J, Vidstrand P, Zatsepin S, 2007a.** Subglacial drainage by groundwater-channel coupling, and the origin of esker systems: Part I – glaciological observations. Quaternary Science Review 26, 1067–1090.

**Boulton G S, Lunn R J, Vidstrand P, Zatsepin S, 2007b.** Subglacial drainage by groundwater-channel coupling, and the origin of esker systems: Part II – theory and simulation of a modern system. Quaternary Science Reviews 26, 1091–1105.

**Bremeer C W, Clark P U, Haggerty R, 2002.** Modelling the subglacial hydrology of the late Pleistocene Lake Michigan Lobe, Laurentide Ice Sheet. GSA Bulletin 114, 665–674.

**Burt T P, Williams P J, 1976.** Hydraulic conductivity in frozen soils. Earth Surface Processes 1, 349–360.

**Carlson A E, Jenson J W, Clark P U, 2007.** Modeling the subglacial hydrology of the James Lobe of the Laurentide Ice Sheet. Quaternary Science Reviews 26, 1384–1397.

**Chan T, Christiansson R, Boulton G S, Ericsson L O, Hartikainen J, Jensen R M, Mas Ivars D, Stanchell W F, Vidstrand P, Wallroth T, 2005.** DECOVALEX III BMT3/BENCHPAR WP4: The thermo-hydro-mechanical responses of a glacial cycle and their potensial implication for deep geological disposal of nuclear fuel waste in a fractured crystalline rock mass. International Journal of Rock Mechanics and Mining Science 42, 805–827.

**Chandler D M, Wadham J L, Lis G P, Cowton T, Sole A, Bartholomew I, Telling J, Nienow P, bagshaw E B, Mair D, Vinen S, Hubbard A, 2013.** Evolution of the subglacial drainage system beneath the Greenland Ice Sheet revealed by tracers. Nature Geoscience 6, 195–198.

**Claesson Liljedahl L, Kontula A, Harper J, Näslund J-O, Selroos J-O, Pitkänen P, Puigdomenech I, Hobbs M, Follin S, Hirschorn S, Kennel L, Marcos N, Ruskeeniemi T, Tullborg E-L, Vidstrand P, 2016.** The Greenland Analogue Project: Final report. SKB TR-14-13, Svensk Kärnbränslehantering AB.

**Clark I D, Douglas M, Raven K, Bottomley D, 2000.** Recharge and preservation of Laurentide glacial melt water in the Canadian Shield, Ground Water 38, 735–742.

**Cohen D, Person M, Wang P, Gable C W, Hutchinson D, Marksamer A, Dugan B, Kooi H, Lizarralde D, Evans L R, Day-Lewis D F, Lane J W, 2010.** Origin and extent of fresh paleowaters on the Atlantic continental shelf, USA. Ground Water 48, 143–158.

**de Marsily G, 1986.** Quantitative hydrogeology: groundwater hydrology for engineers. Orlando: Academic Press.

**Douglas M, Clark I D, M, Raven K, Bottomley D, 2000.** Groundwater mixing dynamics at a Canadian Shield mine. Journal of Hydrology 235, 88–103.

**Dow C F, Kulessa B, Rutt I C, Tsai V C, Pimentel S, Doyle S H, van As D, Lindbäck K, Pettersson R, Jones G A, Hubbard A, 2015.** Modeling of subglacial hydrological development following rapid supraglacial lake drainage. Journal of Geophysical Research: Earth Surface 120, 1127–1147.

**Engström J, Paananen M, Klint K E, 2012.** The Greenland Analogue Project. Geomodel version 1 of Kangerlussuaq area on Western Greenland. Posiva Working Report 2012-10, Posiva Oy, Finland.

**Escher A, 1971.** Geologisk kort over Grønland 1:500000, Kort nr. 3: Søndre Strømfjord – Nûgssuaq. De Nationale Geologiske Undersøgelser for Danmark og Grønland.

**Ferguson G A G, Betcher R N, Grasby S E, 2007.** Hydrogeology of the Winnipeg formation in Manitoba, Canada. Hydrogeology Journal 15, 573–587.

**Fischer U H, Bebiolka A, Brandefelt J, Follin S, Hirschorn S, Jensen M, Keller S, Kennell L, Näslund J-O, Normani S, Selroos J-O, Vidstrand P, 2015.** Radioactive waste under conditions of future ice ages. In Haeberli W, Whiteman C (eds). Snow and ice-related hazards, risks, and disasters. Academic Press, 345–393.

**Flowers G E, Clarke G K C, 2002.** A multicomponent coupled model of glacier hydrology. 1. Theory and synthetic examples. Journal of Geophysical Research: Solid Earth 107, 2287. doi:10.1029/2001JB001122

**Follin S, 2008.** Bedrock hydrogeology Forsmark. Site descriptive modelling, SDM-Site Forsmark. SKB R-08-95, Svensk Kärnbränslehantering AB.

**Follin S, Stigsson M, Rhén I, Engström J, Klint K E, 2011.** Greenland Analogue Project – Hydraulic properties of deformation zones and fracture domains at Forsmark, Laxemar and Olkiluoto for usage together with Geomodel version 1. SKB P-11-26, Svensk Kärnbränslehantering AB.

**Forman S L, 2008.** Little Ice Age and neoglacial landforms at the Inland Ice margin, Isunguata Sermia, Kangerlussuaq, west Greenland. Boreas 36, 341–351.

**French H M, 1996.** The periglacial environment. 2nd ed. Harlow: Longman.

**Glamheden R, Fredriksson A, Röshoff K, Karlsson J, Hakami H, Christiansson R, 2007.** Rock mechanics Forsmark. Site descriptive modelling Forsmark stage 2.2. SKB R-07-31, Svensk Kärnbränslehantering AB.

**Grasby S E, Osadetz K, Betcher R, Render F, 2000.** Reversal of the regional-scale flow system of the Williston basin in response to Pleistocene glaciation. Geology 28, 635–638.

**Haggerty R, Gorelick S M, 1995.** Multiple-rate mass transfer for modelling diffusion and surface reactions in media with pore-scale heterogeneity. Water Resources Research 31, 2383–2400.

**Hakami E, Fredriksson A, Lanaro F, Wrafter J, 2008.** Rock mechanics Laxemar. Site descriptive modelling, SDM-Site Laxemar. SKB R-08-57, Svensk Kärnbränslehantering AB.

**Haldorsen S, Heim M, 1999.** An arctic groundwater system and its dependence upon climatic change: an example from Svalberg. Permafrost and Periglacial Processes 10, 137–149.

**Harper J, Hubbard A , Ruskeeniemi T, Claesson-Liljedahl L, Lehtinen A, Booth A, Brinkerhoff D, Drake H, Dow C, Doyle S, Engström J, Fitzpatrick A, Frape S, Henkemans E, Humphrey N, Johnson J, Jones G, Joughin I, Klint K E, Kukkonen I, Kulessa B, Landowski C, Lindbäck K, Makahnouk M, Meierbachtol T, Pere T, Pedersen K, Pettersson R, Pimentel S, Quincey D, Tullborg E-L, van As D, 2011.** The Greenland Analogue Project. Yearly report 2010. SKB R-11-23, Svensk Kärnbränslehantering AB.

**Harper J, Hubbard A, Ruskeeniemi T, Claesson Liljedahl L, Kontula A, Hobbs M, Brown J, Dirkson A, Dow C, Doyle S, Drake H, Engström J, Fitzpatrick A, Follin S, Frape S, Graly J, Hansson K, Harrington J, Henkemans E, Hirschorn S, Humphrey N, Jansson P, Johnson J, Jones G, Kinnbom P, Kennell L, Klint K E, Liimatainen J, Lindbäck K, Meierbachtol T, Pere T, Pettersson R, Tullborg E-L, van As D, 2016.** The Greenland Analogue Project: Data and processes. SKB R-14-13, Svensk Kärnbränslehantering AB.

**Howat I M, Negrete A, Smith B E, 2014.** The Greenland Ice Sheet Mapping Project (GIMP) land classification and surface elevation data sets. The Cryosphere 8, 1509–1518.

**Hughes T J, 1998.** Ice sheets. New York: Oxford University Press.

**Hökmark H, Lönnqvist M, Fälth B, 2010.** THM-issues in repository rock. Thermal, mechanical, thermo-mechanical and hydro-mechanical evolution of the rock at the Forsmark and Laxemar sites. SKB TR-10-23, Svensk Kärnbränslehantering AB.

**Jansson P, Näslund J-O, Rodhe L, 2007.** Ice sheet hydrology – a review. SKB TR-06-34, Svensk Kärnbränslehantering AB.

**Jaquet O, Siegel P, 2003.** Groundwater flow and transport modelling during a glaciation period. SKB R-03-04, Svensk Kärnbränslehantering AB.

**Jaquet O, Siegel P, 2006.** Regional groundwater flow model for a glaciation scenario. Simpevarp subarea – version 1.2. SKB R-06-100, Svensk Kärnbränslehantering AB.

**Jaquet O, Namah R, Jansson P, 2010.** Groundwater flow modelling under ice sheet conditions Scoping calculations. SKB R-10-46, Svensk Kärnbränslehantering AB.

**Jaquet O, Namah R, Siegel P, Jansson P, 2012.** Groundwater flow modelling under ice sheet conditions in Greenland (phase II). SKB R-12-14, Svensk Kärnbränslehantering AB.

**Kamb B, 1986.** Stress-gradient coupling in glacier flow: III. Exact longitudinal equilibrium equation. Journal of Glaciology, 32, 335–341.

**Kamb B, 1987.** Glacier surge mechanism based on linked cavity configuration of the basal water conduit system. Journal of Geophysical Research: Solid Earth 92, 9083–9100.

**Kane D L, Stein J, 1983.** Water movement into seasonally frozen soils. Water Resources Research 19, 1547–1557.

**Kelly M, 1985.** A review of the Quaternary geology of Western Greenland. In Andrews J T (ed). Quaternary Environments: Eastern Canadian Arctic, Baffin Bay and Western Greenland. Norwich, UK: Geobooks, 525–560.

**King-Clayton L M, Chapman N A, Kautsky F, Svensson N-O, de Marsily G, Ledoux E, 1995.** The central scenario for SITE-94: a climate change scenario. SKI Report 95:42, Statens kärnkraft-inspektion (Swedish Nuclear Power Inspectorate).

**Kleinberg R L, Griffin D D, 2005.** NMR measurements of permafrost: unfrozen water assay, pore-scale distribution of ice, and hydraulic permeability of sediments. Cold Regions Science and Technology 42, 63–77.

**Lemieux J-M, Sudicky E A, Peltier W R, Tarasov L, 2008a.** Simulating the impact of glaciations on continental groundwater flow systems: 1. Relevant processes and model formulation. Journal of Geophysical Research 113, F03017. doi:10.1029/2007JF000928

**Lemieux J-M, Sudicky E A, Peltier W R, Tarasov L, 2008b.** Simulating the impact of glaciations on continental groundwater flow systems: 2. Model application to the Wisconsinian glaciation over the Canadian landscape. Journal of Geophysical Research 113, F03018. doi:10.1029/2007JF000929

**Lemieux J-M, Sudicky E A, Peltier W R, Tarasov L, 2008c.** Dynamics of groundwater recharge and seepage over the Canadian landscape during the Wisconsinian glaciation. Journal of Geophysical Research 113, F01011. doi:10.1029/2007JF000838

**Lindbäck K, Pettersson R, Doyle S H, Helanow C, Jansson P, Savstrup Kristensen S, Hubbard A L, 2014.** High-resolution ice thickness and bed topography of a land-terminating section of the Greenland Ice Sheet. Earth System Science Data Discussions 7, 129–148.

**Lunardini V J, 1988.** Freezing of soil with an unfrozen water content and variable thermal properties. CRREL Report 88-2.

**Lund B, Schmidt P, Hieronymus C, 2009.** Stress evolution and fault stability during the Weichselian glacial cycle. SKB TR-09-15, Svensk Kärnbränslehantering AB.

**Lönnqvist M, Hökmark H, 2010.** Assessment of potential for glacially induced hydraulic jacking at different depths. SKB R-09-35, Svensk Kärnbränslehantering AB.

**Marshall S J, Clark P U, 2002.** Basal temperature evolution of North American ice sheets and implications for the 100-kyr cycle. Geophysical Research Letters 29, 2214, doi:10.1029/2002GL015192.

**Mattila J, 2009.** Constraints on the fault and fracture evolution at the Olkiluoto region. Posiva Working Report 2009-130, Posiva Oy, Finland.

**McEwan T, de Marsily G, 1991.** The potential significance of permafrost to the behaviour off a deep radioactive waste repository. SKI TR 91:8, Statens kärnkraftinspektion (Swedish Nuclear Power Inspectorate).

**Meierbachtol T, Harper J, Humphrey N, 2013.** Basal drainage system response to increasing surface melt on the Greenland ice sheet. Science 341, 777–779.

**Moeller C A, Mickelson D M, Anderson M P, Winguth C, 2007.** Groundwater flow beneath Late Weichselian glacier ice in Nordfjord, Norway. Journal of Glaciology 53, 84–90.

**Mottaghy D, Rath V, 2006.** Latent heat effects in subsurface heat transport modelling and their impact on palaeotemperature reconstructions. Geophysical Journal International 164, 236–245.

**Neuzil C E, 2003.** Hydromechanical coupling in geologic processes. Hydrogeology Journal 11, 41–83.

**Neuzil C E, 2012.** Hydromechanical effects of continental glaciation on groundwater systems. Geofluids 12, 22–37.

**Normani S D, Sykes J F, 2012.** Paleohydrogeologic simulations of Laurentide ice-sheet history on groundwater at the eastern flank of the Michigan Basin. Geofluids 12, 97–122.

**Nye J F, 1973.** Water at the bed of an ice sheet. Proceedings of the Symposium on the hydrology of glaciers, Cambridge, September 1969. IAHS Publication 95, 189–194.

**Paterson W S B, 1994.** The physics of glaciers. 3rd ed. Oxford: Pergamon.

**Person M, McIntosh J, Bense V, Remenda V H, 2007.** Pleistocene hydrology of North America: the role of ice sheets in reorganising groundwater flow systems. Reviews of Geophysics 45. doi:10.1029/2006RG000206

**Piotrowski J A, 1997a.** Subglacial groundwater flow during the last glaciation in north-western Germany. Sedimentary Geology 111, 217–224.

**Piotrowski J A, 1997b.** Subglacial hydrology in north-western Germany during the last glaciation: groundwater flow, tunnel valleys and hydrological cycles. Quaternary Science Reviews 16, 169–185.

**Piotrowski J A, Hermanowski P, Piechota A M, 2009.** Meltwater discharge through the subglacial bed and its land-forming consequences from numerical experiments in the Polish lowland during the last glaciation. Earth Surface Processes and Landforms 34, 481–492.

**Röthlisberger H, 1972.** Water pressure in intra- and subglacial channels. Journal of Glaciology 11, 177–203.

**SKB, 2010.** Climate and climate related issues for safety assessment SR-Site. SKB TR-10-49, Svensk Kärnbränslehantering AB

**Sugden D E, John B S, 1976.** Glaciers and landscape: a geomorphological approach. London: Arnold.

**Svensson U, 1996.** Regional groundwater flow due to an advancing and retreating glacier – scoping calculations. SKB U-96-35, Svensk Kärnbränslehantering AB.

**Svensson U, 1999.** Subglacial groundwater flow at Äspö as governed by basal melting and ice tunnels. SKB R-99-38, Svensk Kärnbränslehantering AB.

**Svensson U, 2001a.** A continuum representation of fracture networks. Part I: Method and basic test cases. Journal of Hydrology 250, 170–186.

**Svensson U, 2001b.** A continuum representation of fracture networks. Part II: application to the Äspö Hard Rock laboratory. Journal of Hydrology 250, 187–205.

**Svensson U, Ferry M, Kuylenstierna H-O, 2010.** DarcyTools version 3.4 – Concepts, methods and equations. SKB R-07-38, Svensk Kärnbränslehantering AB.

**Tarasov L, Peltier W R, 2004.** A geophysically constrained large ensemble analysis of the deglacial history of the North American ice-sheet complex. Quaternary Science Reviews 23, 359–388.

**Tarasov L, Peltier W R, 2007.** Co-evolution of continental ice cover and permafrost extent over the last glacial-interglacial cycle in North America. Journal of Geophysical Research 112, F02S08. doi:10.1029/2006JF000661

**van der Veen C J, 2007.** Fracture propagation as means of rapidly transferring surface meltwater to the base of glaciers. Geophysical Research Letters 34, L01501. doi:10.1029/2006GL028385

**van Tatenhove F G M, van der Meer J J M, Koster E A, 1996.** Implications for deglaciation chronology from the new AMS age determinations in central West Greenland. Quaternary Research 45, 245–253.

**Vidstrand P, Näslund J-O, Hartikainen J, Svensson U, 2007.** Hydrogeological flux scenarios at Forsmark. Generic numerical flow simulations and compilation of climatic information for use in the safety analysis SFR1 SAR-08. SKB R-07-63, Svensk Kärnbränslehantering AB.

**Vidstrand P, Follin S, Zugec N, 2010a.** Groundwater flow modelling of periods with periglacial and glacial climate conditions – Forsmark. SKB R-09-21, Svensk Kärnbränslehantering AB.

**Vidstrand P, Rhén I, Zugec N, 2010b.** Groundwater flow modelling of periods with periglacial and glacial conditions – Laxemar. SKB R-09-25, Svensk Kärnbränslehantering AB.

**Vidstrand P, Follin S, Selroos J-O, Näslund J-O, Rhén I, 2013.** Modeling of groundwater flow at depth in crystalline rock beneath a moving ice-sheet margin, exemplified by the Fennoscandian Shield, Sweden. Hydrogeology Journal 21, 239–255.

**Vidstrand P, Follin S, Selroos J-O, Näslund J-O, 2014.** Groundwater flow modeling of periods with periglacial and glacial climate conditions for the safety assessment of the proposed high level nuclear waste repository site at Forsmark, Sweden. Hydrogeology Journal 22, 1251–1267.

**Walder J S, Fowler A, 1994.** Channelized subglacial drainage over a deformable bed. Journal of Glaciology 40, 3–15.

**Walder J S, Hallet B, 1979.** Geometry of former subglacial water channels and cavities. Journal of Glaciology 23, 335–346.

**Wallroth T, Lokrantz H, Rimsa A, 2010.** The Greenland Analogue Project (GAP). Literature review of hydrogeology/hydrogeochemistry. SKB R-10-34, Svensk Kärnbränslehantering AB.

**Walsh R, Avis J, 2010.** Glacial scenario: groundwater and radionuclide transport studies. NWMO TR-2009-23, Nuclear Waste Management Organization, Canada.

**Wang H F, 2000.** Theory of linear poroelasticity: with applications to geomechanics and hydrogeology. Princeton, NJ: Princeton University Press.

**Weertman J, 1972.** General theory of water flow at the base of a glacier or ice sheet. Reviews of Geophysics 10, 287–333.

**Weidick A, 1968.** Observations on some holocene glacier fluctuations in West Greenland. Copenhagen. (Meddelelser om Grønland 165:6)

**Werder M A, Hewitt I J, Schoof C G, Flowers G E, 2013.** Modeling channelized and distributed subglacial drainage in two dimensions. Journal of Geophysical Research: Earth Surface 118, 2140–2158.

**Willemse N W, Törnqvist T E, 1999.** Holocene century-scale temperature variability from West Greenland lake records. Geology 27, 580–584.

**Williams P J, Smith M W, 1989.** The frozen earth: fundamentals of geocryology. Cambridge: Cambridge University Press.

**Yin Y, Normani S, Sykes J, Barnard M, 2013.** Preliminary hydrogeological modelling of a crystalline rock setting in Western Greenland. NWMO TR-2013-12, Nuclear Waste Management Organization, Cananda.

**Zwally H J, Abdalati W, Herring T, Larson K, Saba J, Steffen K, 2002.** Surface melt-induced acceleration of Greenland ice-sheet flow. Science 297, 218–222.

Arkitektkopia AB, Bromma, 2017

SKB is responsible for managing spent nuclear fuel and radioactive waste produced by the Swedish nuclear power plants such that man and the environment are protected in the near and distant future.

**skb.se**